International Journal of Advances in Telecommunications Electrotechnics, Signals and Systems

a publication of the International Science and Engineering Society

Vol. 3, No. 2
2014

ISSN: 1805-5443

www.ijates.org

I J A T E S²

International Journal of Advances in Telecommunications Electrotechnics, Signals and Systems

a publication of the International Science and Engineering Society

Vol. 3, No. 2, 2014 ISSN: 1805-5443

Aims and Scope

The International Journal of Advances in Telecommunications, Electronics, Signals and Systems (IJATES²) is an all-electronic international scientific journal with the aim to bring the most recent and unpublished research and development results in the area of electronics to the scientific and technical societies, and is supported by the ISES (International Science and Engineering Society, o.s.). The journal's scope covers all the aspects of telecommunication, signal processing, theory and design of circuits and systems for electronics.

The IJATES² is ready to publish experimental and theoretical full papers and letters submitted by prospective authors. Paper submitted for publication must be written in English and must follow a prescribed format. All papers are subjected to a critical peer-review prior to publication.

The IJATES² is an open access journal which means that all content is freely available without charge to the user or his/her institution. Users are allowed to read, download, copy, distribute, print, search, or link to the full texts of the articles in this journal without asking prior permission from the publisher or the author. This journal provides immediate open access to its content on the principle that making research freely available to the public supports a greater global exchange of knowledge.

www.ijates.org

CONTENTS

Vol. 3, No. 2, 2014 ISSN: 1805-5443

Enhancing On-Demand Multicast Routing Protocols using Mobility Prediction in Mobile Ad-hoc Network

Nermin Makhlouf

Abstract— **A Mobile Ad-hoc Network (MANET) is a self-organizing wireless communication network in which mobile devices are based on no infrastructure like base stations or access points. Minimal configuration and quick deployment make ad-hoc networks suitable for emergency situations like disaster recovery or military conflict.**

Since node mobility may cause links to be broken frequently, a very important issue for routing in MANETs is how to set reliable paths which can last as long as possible. To solve this problem, non-random behaviors for the mobility patterns that mobile users exhibit are exploited.

This paper introduces a scheme to improve On-Demand Multicast Routing Protocol (ODMRP) performances by using mobility prediction.

***Keywords*— GPS, LET, MANET, mobility prediction, on-demand routing protocol.**

I. INTRODUCTION

Since a mobile ad-hoc network consists of wireless hosts that may move often, the protocol must adapt to frequent changing network topologies. The increased mobility of ad-hoc nodes presents a challenging issue for protocol design. Various routing schemes have been proposed for ad-hoc networks [1], [2], [3], [4]. In order to improve routing protocol performance, there are two schemes that utilize location information (for instance, obtained using the global positioning system). The first scheme is Location Aided Routing (LAR) that uses location information obtained from the Global Positioning System (GPS) [5], [6] to limit the search for a new path to a smaller request region of the ad-hoc network. Another location-based routing protocol is Distance Routing Effect Algorithm for Mobility (DREAM) [7]. DREAM updates routing table periodically.

Multicasting is one of the most significant areas in the field of networking. With the growing technology and popularity of the internet, applications that need multicasting (e.g., video conferencing) are becoming more prevalent. Multicast plays a main role in ad-hoc networks because of the concept of teams and the need to show data to hold conferences between them [15].

In this paper enhancement of the On-Demand Multicast Routing Protocol using Mobility Prediction ODMRP-MP is presented. ODMRP uses on-demand routing techniques to overcome channel overhead and improve scalability. It uses the concept of forwarding group [8] to build a forwarding mesh for each multicast group. By using a mesh instead of a tree, the disadvantages of multicast trees in mobile wireless networks (e.g., intermittent connectivity, traffic concentration, frequent tree reconfiguration, non-shortest path in a shared tree, etc.) are avoided.

The paper is organized as follows. The second section shows the mechanism used for predicting the Link Expiration Time (LET). The third section presents method to enhance on-demand multicast routing protocol based on mobility prediction. The fourth section describes performance evaluation. The final section is conclusion.

Manuscript received July 30, 2014. Revised August 21, 2014.

Nermin Makhlouf is with the Department of Telecommunications, Brno University of Technology, Czech Republic, e-mail: xmakhl00@stud.feec.vutbr.cz.

II. MOBILITY PREDICTION MECHANISMS

To improve various unicast and multicast ad-hoc routing protocols in [9] a prediction mechanism for link expiration time (LET) between two ad-hoc nodes has been studied. We assume a non-random movement pattern [10]. We also assume that all nodes in the network have their clock synchronized (e.g. by using the GPS clock itself). And two nodes *i* and *j* are within the transmission range of each other. We can calculate the period of time two neighboring nodes will remain connected by using mobility parameters of these two nodes (e.g. speed, direction, etc.). If the nodes *i* and *j* at locations (x_i, y_i) and (x_j, y_j) are moving at speed v_i and v_j respectively, and θ_i and θ_j are the moving directions of nodes *i* and *j*, respectively, then the link expiration time is:

$$D_t = \frac{-(ab + cd) + \sqrt{(a^2 + c^2)r^2 - (ad - bc)^2}}{a^2 + c^2} \quad (1)$$

Where,

$$a = v_i \cos\theta_i - v_j \cos\theta_j$$
$$b = x_i - x_j$$
$$c = v_i \sin\theta_i - v_j \sin\theta_j$$
$$d = y_i - y_j .$$

If the nodes *i* and *j* are traveling at the same speed and the same direction ($v_i = v_j, \theta_i = \theta_j$), the link expiration time is unlimited. After predicting the LETs of all links of a route the minimum value of LETs is the Route Expiration Time (RET). This allows rebuilding route before route failure. The prediction of link expiration time may not be accurate because GPS may not work correctly in particular situations (e.g. indoor, fading, etc.)

doi: 10.11601/ijates.v3i2.91

III. Mobility Prediction based Multicast Routing Protocols

A. On Demand Multicast Routing Protocol with Mobility Prediction (ODMRP-MP)

In ODMRP, the source creates and updates group membership and multicast routes on demand (non-periodically) to reduce the channel overhead. ODMRP depends on the concept of forwarding group [8], [13].

The forwarding group is a set of nodes that is in charge of forwarding multicast data on the shortest paths between any member pairs. It has two cycles: a request cycle and a reply cycle. When a source wants to send packets, it periodically broadcasts the join request, which includes a member advertising packet and data, to the entire network to update the membership information and the routes. When a node receives a non-duplicate join request, it saves the source ID in its routing table and then it rebroadcasts the join request. When a desired multicast receiver receives the join request, it builds a join table which is broadcasted to neighboring nodes. When a node receives the join table it understands that it is on the route to the source in case that the next node ID of one of the entries has the same ID. This node is a part of the forwarding group, thus it builds its own join table which is also propagated to neighboring nods after setting the Forwarding Group Flag (FG Flag). Each part of the forwarding group propagates the join table until it reaches the multicast source via the shortest path. This method updates the routes from sources to receivers and builds the forwarding group. Fig. 1 shows the request and the reply cycles of ODMRP. After building the forwarding group and routes, a source can propagate packets to receivers by elected routes and forwarding. When a node receives the multicast data packet, it forwards the multicast data packet if the following two conditions are true: the multicast packet is not a duplicate, and the setting of the FG-Flag for the multicast group is still available. Nodes in the forwarding group will be non-forwarding nodes if they have not received join tables before their FG-Flag are expired. No control packets need to be sent to join or leave the group.

However, ODMRP discovers multicast routes only in the presence of data packets to be delivered to a multicast destination. Route discovery is based on request and reply cycles where multicast route information is stored in all intermediate nodes on the multicast path.

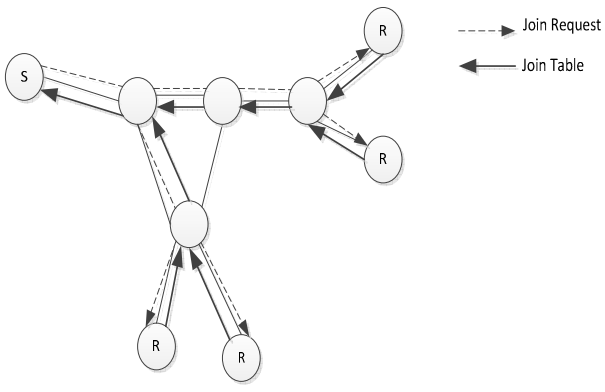

Fig. 1 The request and the reply cycles of ODMRP

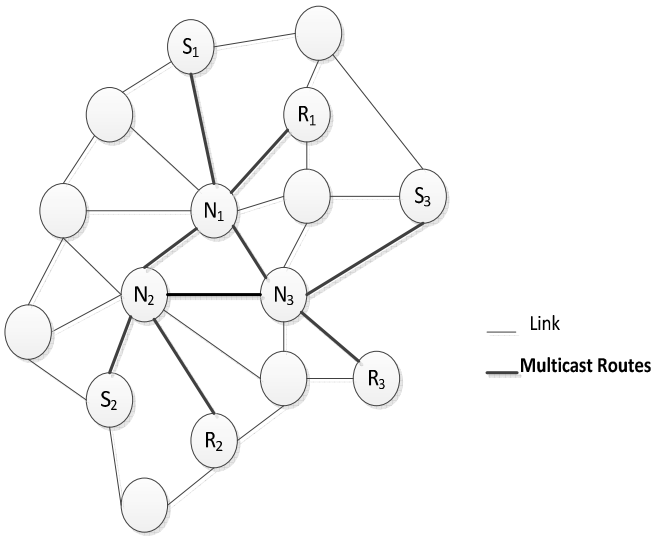

Fig. 2 An example of the ODMRP.

For example, there are three sources (S_1, S_2, S_3) as shown in Fig. 2 These sources send multicast data packets to three receivers (R_1, R_2, R_3) through the forwarding group (N_1, N_2, N_3). The route from S_1 to R_3 is S_1, N_1, N_3, R_3. If the route between N_1 and N_3 is broken, in ODMRP, the route S_1, N_1, N_2, N_3, R_3 will be in exchange for the route S_1, N_1, N_3, R_3. While in a tree configuration, the route from S_1 to R_3 is broken until the tree is reconfigured.

An example of join table forwarding is illustrated in Fig. 3 Multicast receivers R1 and R2 send their join tables to multicast sources S1 and S2 through N1. Multicast receiver R_3 sends its join table to S_1 through N_1 and to S_2 through N_2. When source S_2 wants to send data to R_3, it broadcasts the join request. When node N_2 receives the join request, it saves the source ID in its routing table and then it rebroadcasts the join request. A desired receiver R_3 receives the join request; it builds a join table which is broadcasted to the neighboring nodes. When an intermediate node N_2 receives the join table of R_3, it sets the FG-Flag and builds its join table because the next node ID of one of the entries is the same of its ID.

Note that the channel overhead is decreased in the case where node N1 broadcasts the join table once even though it receives three join tables from three receivers R1, R2, R3

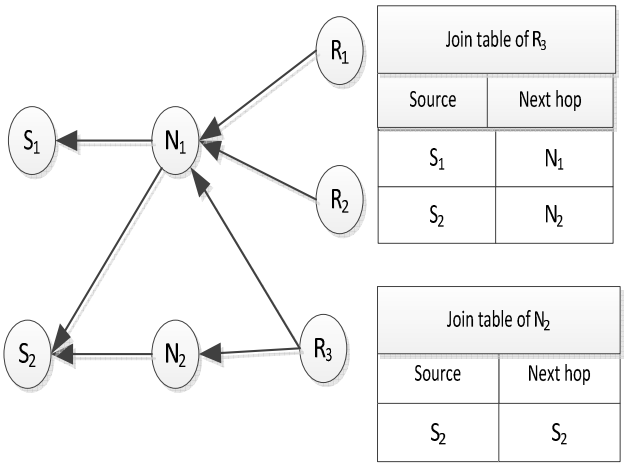

Fig. 3 An example of a join table forwarding.

because these multicast receivers have the same links to the source. ODMRP requires periodic flooding of join request to build and refresh routes which often causes contention and collisions.

Thus it is important to find the optimal flooding interval. Here a scheme adapts the flooding interval to mobility and location information.

B. *Applying mobility prediction*

We predict the period of time two neighboring nodes will remain connected by using mobility parameters of these two nodes provided by GPS [11]. With the predicted time of route disconnection, join request is only flooded when route breaks of ongoing data sessions are imminent. A join request is tailed by the location, speed and direction of the source. The source sets the minimum LET field to the maximum LET value. The neighboring node, which receives a join request, predicts the link expiration time between itself and the previous hop using the equation (1).

It rebroadcasts the join request, but this join request will include the minimum between this value and the MIN LET indicated by the receiving join request, this minimum value is the Rout Expiration Time (RET). The node also updates the location and mobility information field according to its own information. If a forwarding group node receives multiple Join tables with different RET values from the same source to multiple receivers, it selects the minimum RET among them and sends its own join table with the chosen RET value attached. Then the source can build new routes by flooding a join request when route breaks of ongoing data sessions are imminent (i.e. before the minimum RET approaches). And receivers only send Join Tables after receiving join request.

The selection of the MIN REFRESH INTERVAL and the MAX REFRESH INTERVAL should be adaptive to network situations (e.g., traffic type, traffic load, mobility pattern, mobility speed, channel capacity, etc.)

In this scheme, instead of using the minimum delay path, we can choose the most stable route (i.e. the one with the largest RET). An example of route selection algorithms is presented in Fig. 4. Two routes are available from the source S to the receiver R. Route 1 has a path of (S-A-B-C-R) and route 2 has a path of (S-A-D-C-R). The route expiration time of route 1 is 2 (min.(3; 2;4; 5)= 2) while that of route 2 is 4 (min.(3; 5; 1;5)=1). The receiver selects the route with the maximum RET, and hence route 1 is selected.

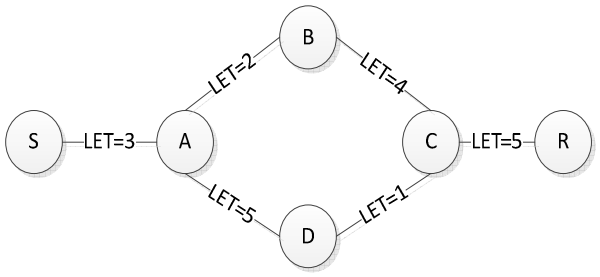

Fig. 4 Route selection example

The multicast receiver should waits for a convenient period of time to receive all possible routes and then the route which has the maximum RET is selected to be included in a join table.

C. *The prediction error*

The route expiration time prediction could become incorrect because a node can accelerate, decelerate and change its direction while it is traveling. Also the mobility information obtained from GPS may not always be accurate.
If we suppose that there is no sudden change of direction and the mobility information obtained from GPS is accurate, the predicted route expiration time of a node could be always accurate.

IV. PERFORMANCE EVALUATION

The simulator has been implemented within the Global Mobile Simulation (GloMoSim) library [14]. The simulated environment consists of 50 wireless mobile nodes roaming in a 1000 meters x 1000 meters flat space for 600 seconds of simulated time. The radio transmission range is 250 meters and channel capacity was 2 Mbit/sec. each packet has a payload of 512 bytes Mbits/sec.
Random waypoint model [12] is used as the mobility model. It means that a node randomly selects a destination and moves towards that destination at a predefined speed. In the MAC layer we use Carrier Sense Multiple Access/Collision Avoidance (CSMA/CA) scheme with acknowledgments.
In order to evaluate ODMRP, we use the following metrics:
Packet Delivery Ratio (PDR) as a function of speed: the ratio of data packets that are successfully delivered to a destination compared to the number of data packets that have been sent out by the sender when the speed varies from 0 to 20 km/h. Mathematically, PDR can be defined as:

$$PDR = \frac{\sum \text{data packets received}}{\sum \text{data packets sent}} \quad (2)$$

Number of Total packets transmitted per data packet delivered (NT): The number of all packets (i.e. join requests, join tables, data, and active acknowledgments) packets transmitted divided by the number of data packet delivered to destinations when the speed varies from 0 to 20 km/h. This measure shows the efficiency in terms of channel access. Mathematically, it can be defined as:

$$NT = \frac{\sum \text{all packets transmitted}}{\sum \text{data packets delivered}} \quad (3)$$

Fig. 5 shows the packet delivery ratio as a function of mobility speed. A comparison was made with ODMRP and ODMRP with Mobility Prediction (ODMRP-MP).

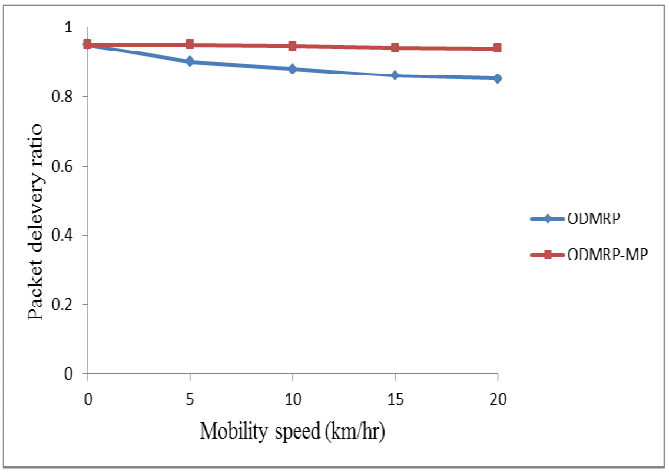

Fig. 5 Packet Delivery Ratio (PDR) as a function of speed

We inferred that ODMRP-MP is more effective compared to ODMRP because ODMRP-MP has a very high packet delivery ratio (over 90%) regardless of speed. While in ODMRP the packet delivery degrades rapidly by the increase in the speed. This result is logical because ODMPR-MP reconstructs the routes before topology changes, thus most data are received without being lost.

Fig. 6 shows the number of total packets transmitted per data packet delivered as a function of mobility speed for both ODMRP and ODMRP-MP. In ODMRP-MP, in order to adapt to the increasing speed, more control packets need to be sent. ODMRP-MP therefore delivers a high part of the data to destinations regardless of speed. Thus the number of total packets transmitted per data packet delivered increases with mobility speed. The number of total packets transmitted per data packet delivered for ODMRP almost does not change with speed.

V. Conclusion

In summary, we have presented the use of mobility prediction with ODMRP to overcome channel overhead and to improve scalability. ODMRP-MP predicts the time of route disconnection, thus it reconstructs the routs when route breaks of ongoing data sessions are imminent (i.e. before the minimum RET approaches).

It uses the concept of forwarding group [7] to build a forwarding mesh for each multicast group.

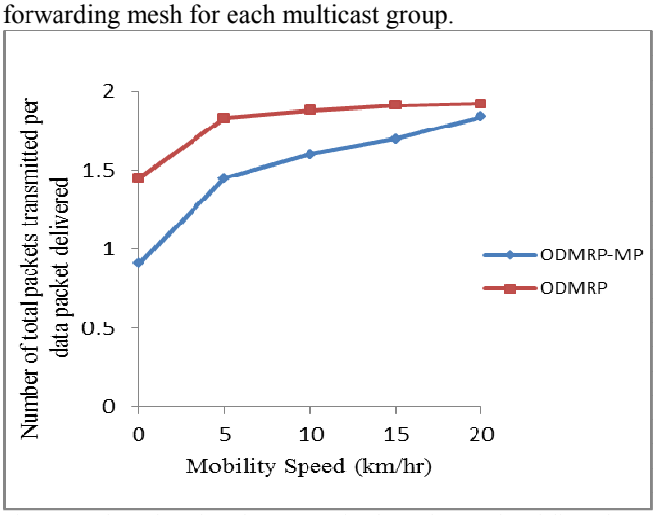

Fig. 6 Number of total packets transmitted per data packet delivered as a function of speed

Compared with trees the disadvantages of multicast trees in mobile wireless networks (e.g., intermittent connectivity, traffic concentration, frequent tree reconfiguration, non-shortest path in a shared tree, etc.) are avoided. According to simulation results with mobility prediction enhancements, more data packets were delivered to destinations. The control packets were used more efficiently.

Acknowledgment

This research is funded by project OPVK CZ.1.07/2.2.00/28.0062 "Joint activities of BUT and VSB-TUO while creating the content of accredited technical courses in ICT".

References

[1] M. S. Corson and A. Ephremides, "A distributed routing algorithm for mobile wireless networks," *Wireless Networks,* vol. 1, no. 1, pp. 61-81, 1995.

[2] S. Murthy and J. J. Garcia-Luna-Aceves, "An efficient routing protocol for wireless networks," *Mobile Networks and Applications,* vol. 1, no. 1, pp. 183-197, 1996.

[3] C.-K. Toh, "Associativity-Based Routing for Ad-hoc Mobile Networks," *Wireless Personal Communications,* vol. 4, no. 2, pp. 103-139, 1997.

[4] C. E. Perkins and E. M. Royer, "Ad-hoc On Demand Distance Vector Routing," in *IEEE WMCSA 99*, New Orleans, 1999.

[5] E. D. Kaplan and C. Hegarty, Understanding GPS: Principles and Applications, Second Edition, Boston: Artech House, 2005.

[6] S. Basagni, I. Chlamtac, V. R. Syrotiuk and B. A. Woodward, "A distance routing effect algorithm for mobility (DREAM)," in *the 4th annual ACM/IEEE international conference on Mobile computing and networking*, New York, 1998.

[7] M. S. Grewal, L. R. Weill and A. P. Andrews, Global positioning systems, inertial navigation, and integration, 2nd Edition, new gersey: Wiley, 2007.

[8] W. Su and M. Gerla, "IPv6 flow handoff in ad-hoc wireless networks using mobility prediction," in *Global Telecommunications Conference*, Rio de Janeireo, 1999.

[9] T. S. Rappaport, Wireless Communications: Principles and Practice, Prentice Hall, 1995.

[10] C.-C. Chiang, M. Gerla and L. Zhang, "Forwarding Group Multicast Protocol (FGMP) for Multihop, Mobile Wireless Networks," *Cluster Computing,* vol. 1, no. 2, pp. 187-196, 1998.

[11] E. D. Kaplan and C. J. Hegarty, Understanding the GPS: Principles and Applications, Artech House, 2006.

[12] C. Bettstetter, G. Resta and P. Santi, "The node distribution of the random waypoint mobility model for wireless ad-hoc networks," *Mobile Computing, IEEE Transactions on,* vol. 2, no. 3, pp. 257 - 269, 2003.

[13] S.-J. Lee, W. Su and M. Gerla, "On-Demand Multicast Routing Protocol in Multihop Wireless Mobile Networks," *Mobile Networks and Applications,* vol. 7, no. 6, pp. 441-453, 2002.

[14] C. E. Perkins and E. M. Royer, "Ad-hoc On Demand Distance Vector Routing," in *IEEE WMCSA 99*, New Orleans, 1999.

[15] Z. Wang, Y. Liang and L. Wang, "Multicast in Mobile ad-hoc Networks," *Computer And Computing Technologies In Agriculture,* vol. 258, no. 1, pp. 151-164, 2008.

Nermin Makhlouf was born in Damascus 1986. She was awarded the Degree of License in Electrical Engineering, department of Electronics and Telecommunications Engineering, Damascus University, Damascus, Syria in 2009.

She is a postgraduate student at Department of Telecommunications, Brno University of Technology, Brno, Czech Republic

Her research work has been concentrated on prediction of movement of wireless nodes in mobile ad-hoc networks MANETs. Recently she has also been concerned with routing protocols in mobile ad-hoc networks and how to overcome the interference and collision among nodes in such networks.

High Speed Level Converters With Short Circuit Current Reduction

Adipudi Bala Tripura Sundari and Avireni Srinivasulu, *SMIEEE*

***Abstract*—The level converter is used as interface between low voltages to high voltage boundary. The efficient level converter has less power consumption and less delay are the design considerations of the level shifter. In this paper two new CMOS level converters are presented with high driving capability and low propagation delay. The proposed level converters are simulated using Cadence software with 0.18 µm CMOS technology. The simulation result shows that the proposed circuits have less propagation delay than existing ones. The circuits are simulated with different load capacitor values and different voltages. The proposed level converters operate for different input pulse signal amplitude values are +0.8 V, +1 V, +1.2 V and V_{DDH} values of +1.8 V and +3.3 V.**

Keywords*— *High speed, level converter, propagation delay, power converters, short circuit current

I. Introduction

Transistor sizes in CMOS process technology lead to many advantages in terms of speed and functionality of the level converter [1]-[11]. For maintaining reliability of system supply voltages come down when the size of the transistor is reduced. Level shifter is used in multi supply voltage systems where voltage difference problem exist. Level shifters are used in aero space systems, MEMS, power converters, and in microprocessors [12]-[21].

Conventional voltage level converter [2] is shown in Fig. 1. A low level voltage input signal V_i is applied to the transistor T_1 and complementary input signal is applied to the transistor T_2. The high level voltage output signals (V_{DDH}) are obtained at the node V_{op} and V_{on}. The input signal V_i is high transistor T_1 is ON and T_2 is OFF then the node V_{op} becomes High. V_{op} node decreases from High (V_{DDH}) to Low when the input signal changing from High (V_{DDH}) to Low. Transistor T_1 has to sink the load discharge current and extra short circuit current from T_3. The aspect ratios of PMOS transistors are larger than NMOS transistors because PMOS transistors have less transconductance. This requires large sized NMOS transistors to sink the PMOS current, it increases the short circuit currents. Short circuit currents increase the signal to noise ratio due to the impedance of supply rails.

Manuscript received July 6, 2014, revised September 22, 2014.

Adipudi Bala Tripura Sundari is with the Department of Electronics & Communication Engineering, VFSTR University (Vignan University), Vadlamudi-522213, Guntur, Andhra Pradesh, INDIA.

Avireni Srinivasulu is with the Department of Electronics & Communication Engineering, VFSTR University (Vignan University), Vadlamudi-522213, Guntur, Andhra Pradesh, INDIA. (Mobile: +91 9502223336; Fax No: +91 863 2534468; e-mail: avireni_s@yahoo.com (or) avireni@ieee.org).

The circuit presented in [3] is shown in Fig. 2. When the input V_i and output V_o both are low, then T_2 is ON. Input V_i goes high, transistor T_3 cannot OFF instantly, because its source is connected to the voltage V_{DDH} and gate terminal is connected to voltage V_{DDL}. As a result transistor T_1 sinks the short circuit current from the transistor T_3. Transistor T_2 acts as supply voltage switch for transistors T_3 and T_1. T_2 acts as high resistance switch, hence the input at the gate of T_2 increases slowly.

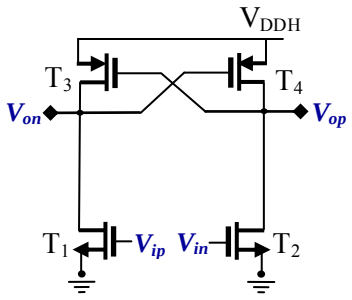

Fig. 1. Conventional voltage level converter [2].

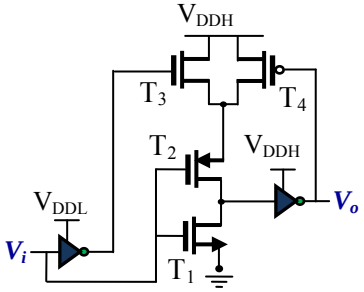

Fig. 2. Conventional voltage level converter [3].

A sub threshold to the above threshold level converter [4] is shown in Fig. 3. This circuit has two stages. First stage uses the cross coupled inverter configuration with NMOS diode connected transistor on top. Second stage is the DCVS logic inverter used for achieving full swing. This design is not useful for high speed, because the second stage of this design affected by short circuit current problem. Second stage of the circuit is DCVSL inverter, the gate of one pull up transistor (T_7) is connected to drain of another pull up transistor (T_8), so short circuit current flows in the circuit when the pull up transistors (T_7 and T_8) are OFF. So propagation delay is increased because the circuit pulls down slowly. The circuit in [4] has higher delay values for 500 mV. This circuit is not used for external loads because it is self loaded.

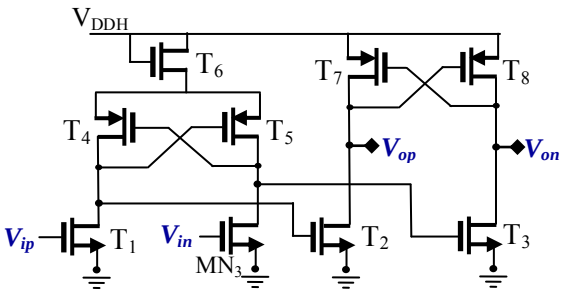

Fig. 3. Conventional voltage level converter [4].

Another Level converter presented in [5] is shown in Fig. 4. Its speed increased than [4] by inserting PMOS diode connected transistors. The diode connected transistors T_3 and T_4 are used to limit the leakage current from pull up transistors T_1 and T_2. This increases the speed of the circuit than Fig. 3. A voltage drop nearly equal to threshold voltage V_{th} occurs in PMOS transistor T_3 or T_4 helps to quickly turn ON the PMOS transistor T_1 or T_2 when these are OFF. The diode drop reduces the output swing; to increase the swing additional transistors T_5 and T_8 are added to pull down the output to low voltage level. The diode connected transistors are used to limit the short circuit current and to improve the speed performance. To reduce the short circuit current further an additional feature is added in [6] hybrid level converter.

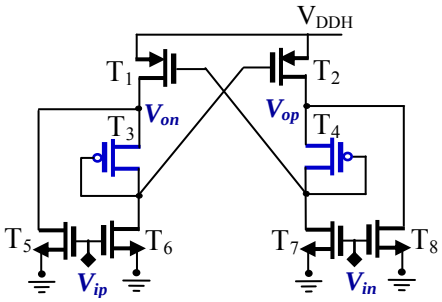

Fig. 4. Conventional diodes based voltage level converter [5].

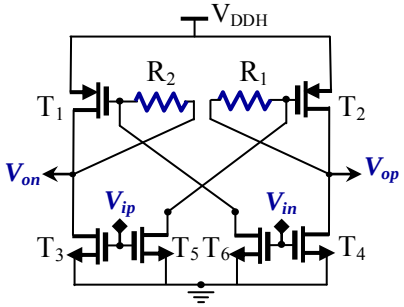

Fig. 5. Conventional voltage level converter with resistors to reduce short circuit current [6].

In Fig. 5 [6] a technique is introduced to reduce the short circuit current. In this technique the PMOS latch is modified by adding resistors R_1 and R_2. These resistances are replaced by NMOS transistors. Transistors T_5 and T_6 are used to minimize the short circuit current. Gate of each PMOS pull up transistor is separated by drain of other PMOS transistor with a resistance. The gate of PMOS transistor is pulled down by NMOS transistors T_5 and T_6 simultaneously. Resistors block the short current from transistors T_1 and T_2. Because of that PMOS transistors (T_1 and T_2) are pulled down quickly.

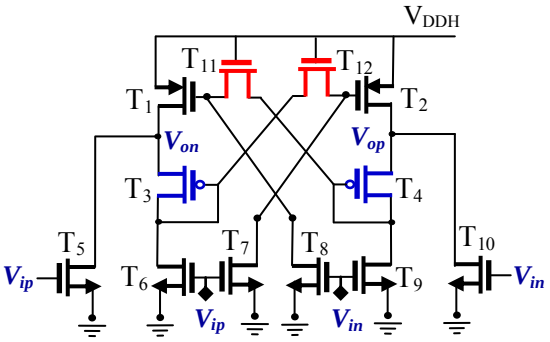

Fig. 6. Conventional hybrid voltage level converter [6].

For achieving high speeds high resistance is useful. When the resistance is high it perfectly blocks the short circuit current from transistors T_1 and T_2. The circuit presented in Fig. 6 [6] is implemented by combining resistive technique (Fig. 5) and diode technique (Fig. 4) in [5]. The final circuit implementation is shown in Fig. 6.

When V_{op} is high and V_{on} is low in Fig. 6 the gate of the transistor T_1 is high where as T_1 is completely OFF. Hence T_{11} has high resistance which helps to pull down the transistor T_1. The gate of T_2 is connected to ground so T_{12} has low resistance to pull up the transistor T_2. Then the output V_{op} become low and V_{on} become high. In this state the gate of the transistor T_2 is high when T_2 is completely OFF. Hence T_{12} has high resistance this is helped to pull down the transistor T_2. The gate of T_1 is connected to ground so T_{11} has low resistance to pull up the transistor T_2. Then V_{op} become high and V_{on} become low. Transistors T_9 and T_{10} are used to minimize the leakage current at pull up transistors T_1 and T_2.

II. Proposed Level Converter Circuits

In the proposed circuits the resistors implemented by using NMOS transistors shown in Fig. 6 [6] are replaced by PMOS transistors and diode connected transistors are also replaced by PMOS transistors used as resistors to quickly pull up the transistors T_1 and T_2 in proposed voltage level converter circuit-I. To block the short circuit current two methods are preferred. One method is to increase the aspect ratios of NMOS transistors T_{11} and T_{12}. Due to the increased aspect ratios of the NMOS transistors area and power consumption of the level converter are increased. Another method is to use the PMOS transistors as resistors. Because PMOS transistors have higher resistance compared to NMOS transistors. The resistance must be high for achieving lesser delay values. If the resistance is high the short circuit flows into the pull up transistors is blocked before the gate terminal and that short circuit current is minimized through the transistors T_7 and T_8. The proposed level converter circuit-I is as shown in Fig. 7.

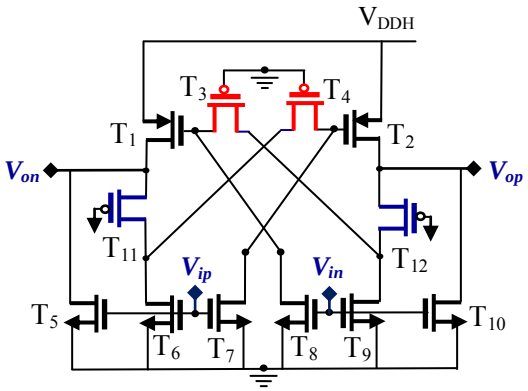

Fig. 7. Proposed voltage level converter-I.

When V_{op} is high and V_{on} is low in Fig. 7, the gate of the transistor T_1 is high whereas T_1 is completely OFF. Hence T_3 has high resistance this is helped to pull down the transistor T_1. The gate of T_2 is connected to ground so T_4 has low resistance to pull up the transistor T_2. Then the output V_{op} becomes low and V_{on} high. In this state the gate of the transistor T_2 is high, when T_2 is completely OFF. Hence T_4 has high resistance this is helped to pull down the transistor T_2. The gate of T_1 is connected to low voltage so T_3 has low resistance to pull up the transistor T_2. Then V_{op} become high and V_{on} become low. Transistors T_7 and T_8 are used to minimize the leakage current at pull up transistors T_1 and T_2. The input V_{ip} is high where transistor T_2 and T_7 are ON. The short circuit current flowing from the transistor T_2 is minimized through T_7. The input V_{ip} is low then transistor T_1 and T_8 are ON. The short circuit current flowing from the transistor T_1 is minimized through T_8. When the input voltage is in transition the operation of the circuit is explained in 3 regions.

Region 1: In region 1 the input V_{ip} is $0 \le V_{ip} \le V_{DDL}$ (where V_{DDL} is the HIGH logic level applied at the input of the level converter) T_1 is ON and T_2 is OFF and a short circuit current flows from the transistor T_2. Transistor T_3 blocks that short circuit current flowing from T_2. If a small amount of short circuit current crosses the transistor T_3 then that is grounded through the transistor T_8.

Region 2: In region 2 the input V_{ip} is equal to $V_{DDL}/2$ all the PMOS and NMOS transistors are ON. No short circuit current flows from the PMOS pull up transistors because both the pull up transistors ON. The node V_{op} raised from 0 to $V_{DDH}/2$ and the V_{on} falls from V_{DDH} to $V_{DDH}/2$.

Region 3: In region 3 the input V_{ip} is $V_{DDL}/2 \le V_{ip} \le V_{DDL}$ (where V_{DDL} is the HIGH logic level applied at the input of the level converter) T_2 is ON and T_1 is OFF and a short circuit current flows from the transistor T_1. Transistor T_4 blocks that short circuit current flowing from T_2. If a small amount of short circuit current crosses the transistor T_4 then that is grounded through the transistor T_9.

When short circuit current in the circuit is reduced the PMOS transistors quickly pulled down to LOW voltage level so response time of the output node V_{OP} is increased. So delay of the circuit is reduced.

T_{11} and T_{12} transistors are used as load helps to quickly turn ON the PMOS transistors. Transistors T_{11} and T_{12} are used to quickly pull up the output nodes V_{op} and V_{on} due to that raise time of the level converter is reduced. The proposed level converter circuit-II is as shown in Fig. 8.

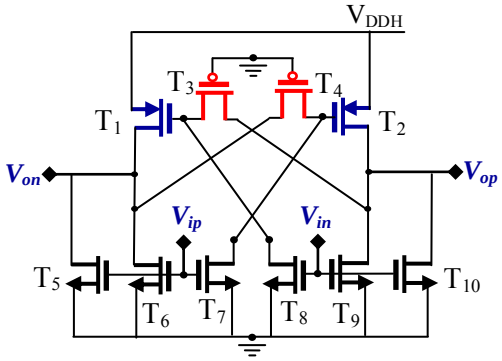

Fig. 8. Proposed voltage level converter-II.

When V_{op} is high and V_{on} is low in Fig. 8 the gate of the transistor T_1 is high so T_1 is completely OFF. Hence T_3 has high resistance which helps to pull down the transistor T_1. The gate of T_2 is connected to ground so T_4 has low resistance to pull up the transistor T_2. Then the output V_{op} become low and V_{on} become high. In this state the gate of the transistor T_2 is high so T_2 is completely OFF. Hence T_4 has high resistance which helps to pull down the transistor T_2. The gate of T_1 is connected to ground so that T_3 has low resistance to pull up the transistor T_2. Then V_{op} become high and V_{on} become low. Transistors T_7 and T_8 are used to minimize the leakage current at pull up transistors T_1 and T_2. When the input V_{ip} is high then transistor T_2 and T_7 are ON. The short circuit current flowing from the transistor T_2 is minimized through T_7. The input V_{ip} is low then transistor T_1 and T_8 are ON. The short circuit current flowing from the transistor T_1 is minimized through T_8. When the input signal is in transition the operation of the Fig. 8 is same as explained in the Fig. 7. T_5 and T_6 transistors are removed in Fig. 8 (proposed level converter circuit-II) to improve delay performance because a voltage drop V_{th} exists in T_5 and T_6 due to that the transistors T_1 and T_2 in Fig. 7 are not completely OFF, so delay of the circuit is increased. When the transistors T_{11} and T_{12} in Fig. 8 are removed T_1 and T_2 takes more time to pull up then raise time is slightly increased and fall time is reduced because no voltage drop exist in Fig. 8.

III. Simulation Results

The circuits are simulated for range of input pulse amplitudes of 0.8 V, 1 V and 1.2 V with the supply voltages of V_{DDH} = 1.8 V and 3.3 V using gpdk 180 nm CMOS technology at a frequency of 5 KHz.

TABLE I. Pulse Input Parameters

S.No	voltage-1	0.8 V, 1 V, 1.2 V
1.	voltage-2	0 V
2.	delay time	2 ns
3.	raise time	1 ns
4.	fall time	1 ns

The simulated input and output waveforms for Fig. 7 are shown in Fig. 9 and Fig. 13. And the simulated input and output waveforms for Fig. 8 are shown in Fig. 10 and Fig. 14. The simulated DC responses for Fig.7 are shown in Fig. 11 and Fig. 15 and the simulated DC responses for Fig. 8 are

shown in Fig. 12 and Fig. 16. The supply voltages are V_{DDH}=1.8 V, 3.3 V and input pulse amplitude of 1 V. Table-I represent the parameters of the pulse input applied at the input V_{ip} of the level converters. Table-II represents the aspect ratios of the transistors used in the implementation of proposed level converters.

TABLE II. ASPECT RATIOS

Transistor	Proposed level converter-I (Fig. 7)	Proposed level converter-II (Fig. 8)
	W (µm)/L (µm)	W (µm)/L (µm)
T_1,T_2,T_6,T_7,T_8,T_9	16/0.18	16/0.18
T_3,T_4	0.4/0.18	0.4/0.18
T_5,T_{10}	8/0.18	8/0.18
T_{11},T_{12}	40/0.18	-

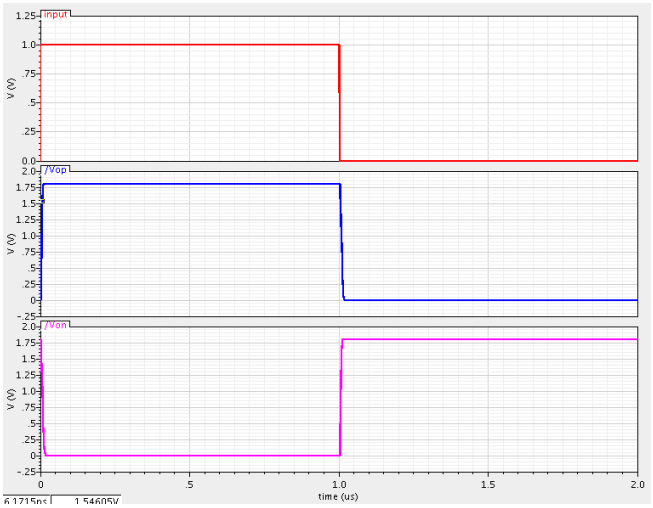

Fig. 9. Simulated input and output waveforms of Fig. 7 with load capacitance C_L=2 pF (Supply rail voltage V_{DDH}=1.8 V and input pulse amplitude=1 V).

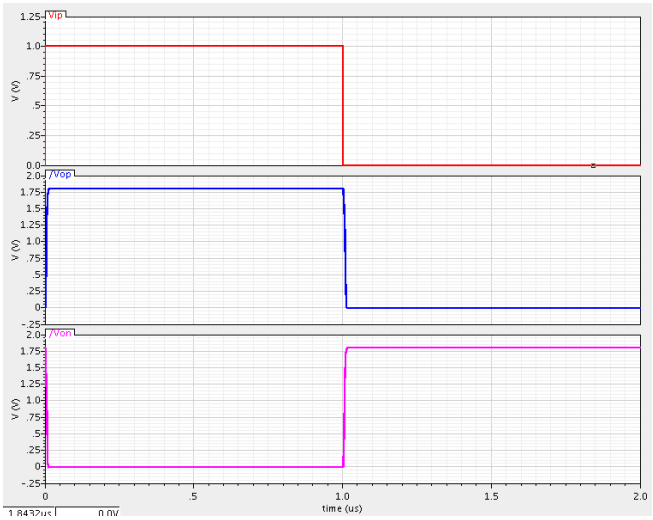

Fig. 10. Simulated input and output waveforms of Fig. 8 with load capacitance C_L=2 pF (Supply rail voltage V_{DDH}=1.8 V and input pulse amplitude=1 V).

Table III represents the comparison of simulated propagation delay values for proposed level converters with diodes based voltage level converter Fig. 4 and hybrid voltage level converter Fig. 6. In this table load capacitor values are varied from 2 pF to 25 pF, with input pulse amplitude of 1 V and frequency of 500 KHz. From table I it is clearly understand that there is a significant reduction of delay in the proposed level converters compared to existing circuits.

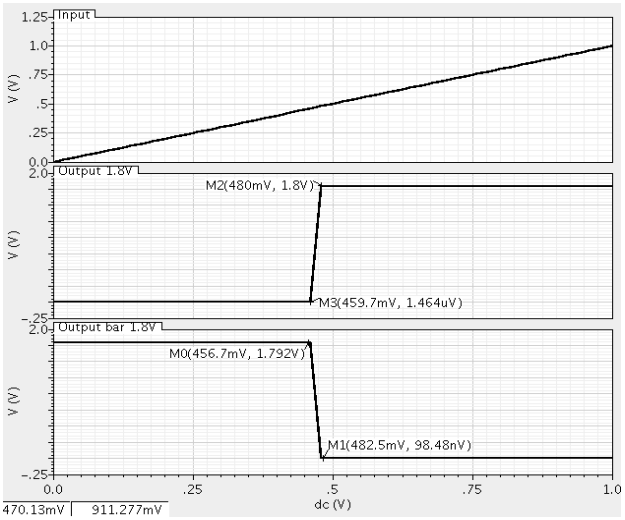

Fig. 11 Simulated DC response of Fig. 7 with load capacitance C_L=2 pF (Supply rail voltage V_{DDH}=1.8 V and input pulse amplitude=1 V).

Table IV represents the simulated values of propagation delay, raise time and fall time for Fig. 7 for different input pulse amplitude values (0.8 V, 1 V, and 1.2 V) and supply voltages V_{DDH} = 1.8 V and 3.3 V with different load capacitor values ranging from 5 pF to 15 pF. Table V represents the simulated values of propagation delay, raise time and fall time for Fig. 8 for different input pulse amplitude values (0.8 V, 1 V, and 1.2 V) and supply voltages V_{DDH} = 1.8 V and 3.3 V with different load capacitor values ranging from 5 pF to 15 pF.

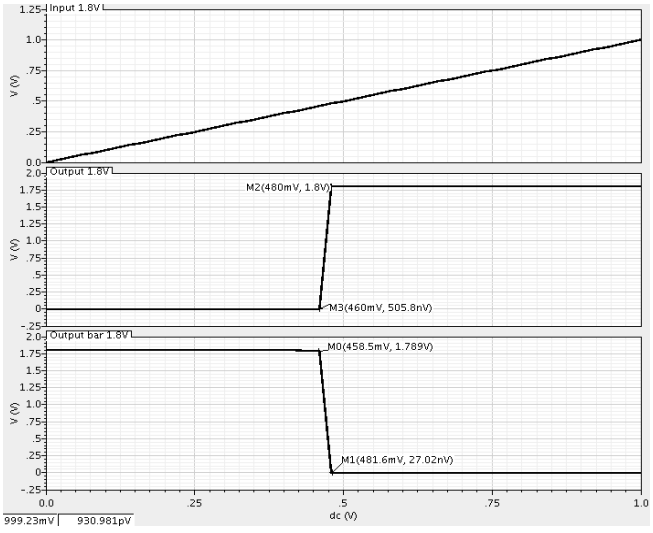

Fig. 12 Simulated DC response of Fig. 8 with load capacitance CL=2 pF (Supply rail voltage V_{DDH}=1.8 V and input pulse amplitude=1 V).

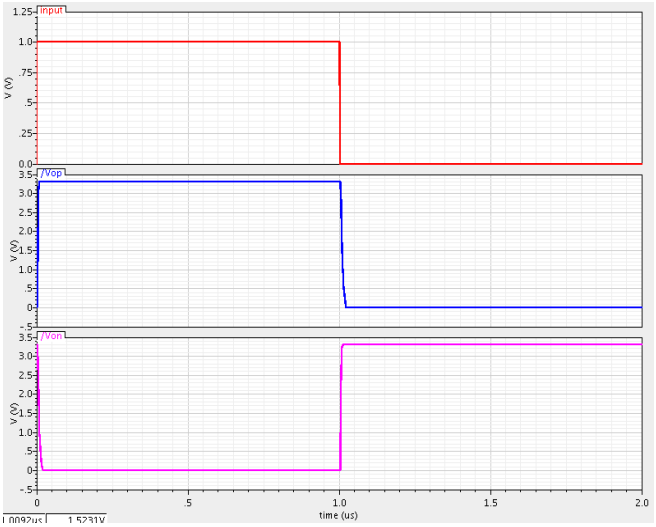

Fig. 13 Simulated input and output waveforms of Fig. 7 with load capacitance C_L=2 pF (Supply rail voltage V_{DDH}=3.3 V and input pulse amplitude=1 V).

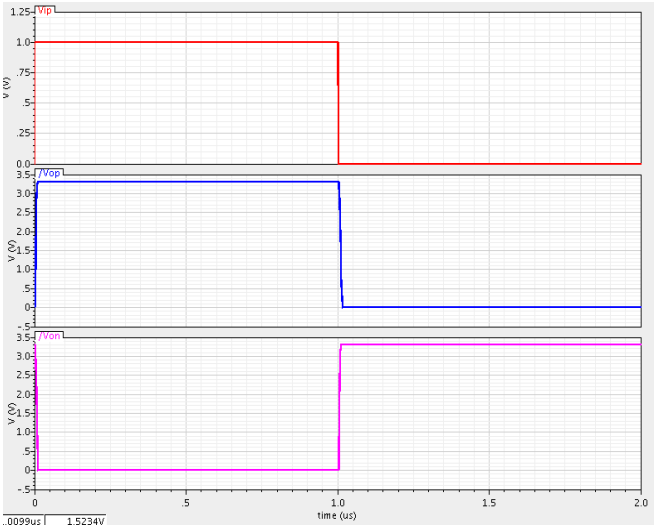

Fig. 14. Simulated input and output waveforms of Fig. 8 with load capacitance C_L=2 pF (Supply rail voltage V_{DDH}=3.3 V and input pulse amplitude=1 V).

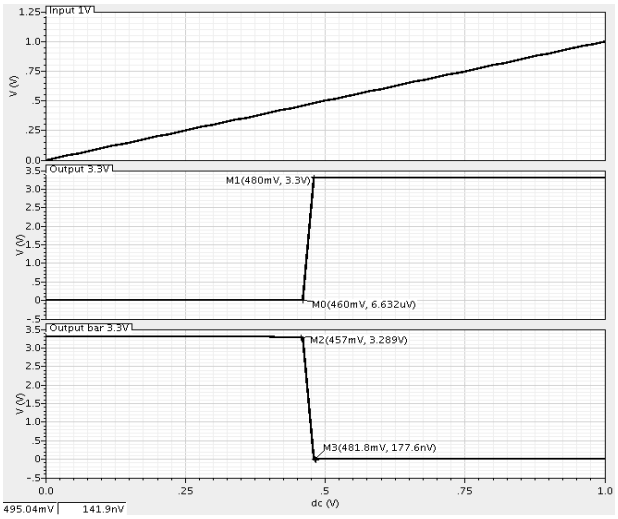

Fig. 15 Simulated DC response of Fig. 7 with load capacitance C_L=2 pF (Supply rail voltage V_{DDH}=3.3 V and input pulse amplitude=1 V).

Figure. 17 and 18 represents propagation delay comparison of proposed level converters and conventional level converters for different input pulse amplitudes ranging from 0.6 V to 1.4 V with supply voltages V_{DDH}=1.8 V and 3.3 V respectively. From Fig. 17 and 18 it is clearly understand that the proposed circuits have better speed performance than Fig. 4 and Fig. 6. When the input voltage amplitude is increasing speed performance of the circuit is increased. At lower supply voltages the speed of Fig. 4 and Fig. 6 is less compared with proposed circuits.

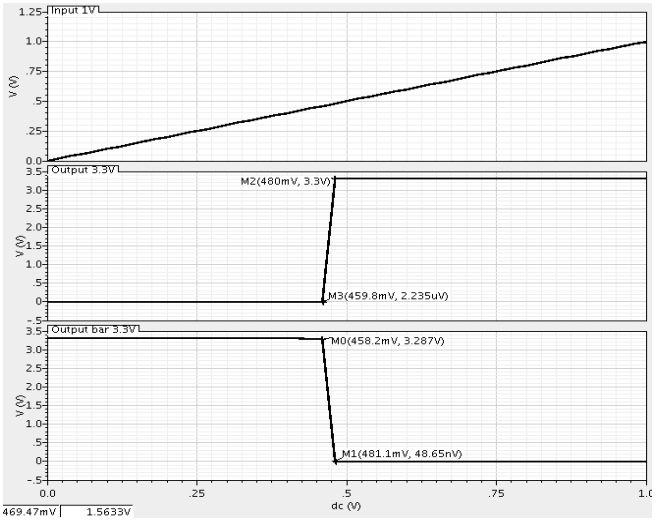

Fig. 16 Simulated DC response of Fig. 8 with load capacitance C_L=2 pF (Supply rail voltage V_{DDH}=3.3 V and input pulse amplitude=1 V).

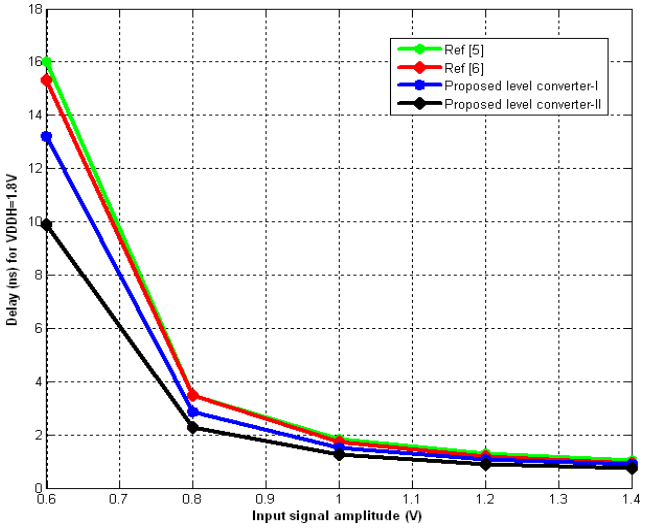

Fig. 17. Proposed level converters and conventional level converters propagation delay comparison for different input pulse amplitudes with supply voltage V_{DDH}=1.8 V.

Figure. 19 and 20 represents propagation delay comparison of proposed level converters and conventional level converters for different loading conditions with supply voltages V_{DDH}=1.8 V and 3.3 V respectively. When the load capacitor is increasing speed of the circuit is decreased. For V_{DDH} of 3.3 V Fig. 4 shows better performance than Fig. 6.

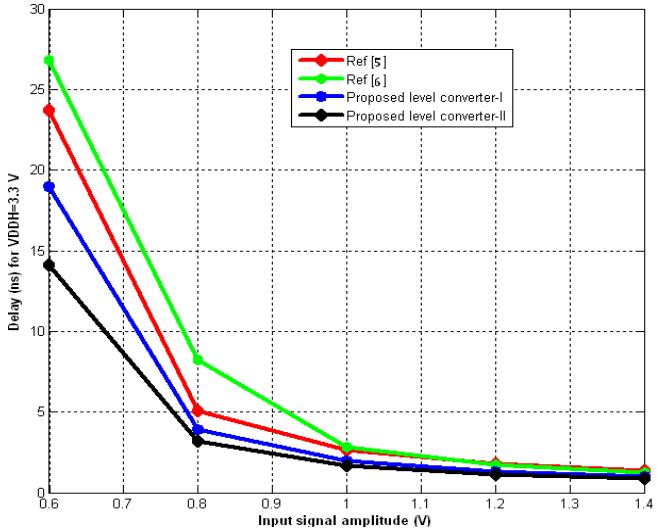

Fig. 18. Proposed level converters and conventional level converters propagation delay comparison for different input pulse amplitudes with supply voltage V_{DDH}=3.3 V.

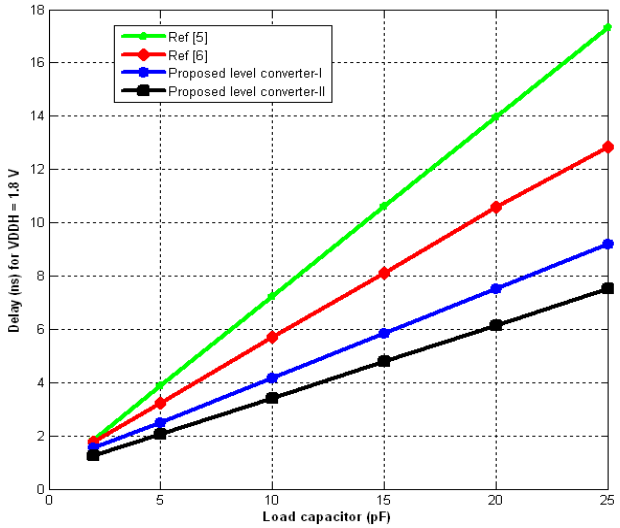

Fig. 19. Proposed level converters and conventional level converters propagation delay comparison for different loading conditions with supply voltage V_{DDH}=1.8V.

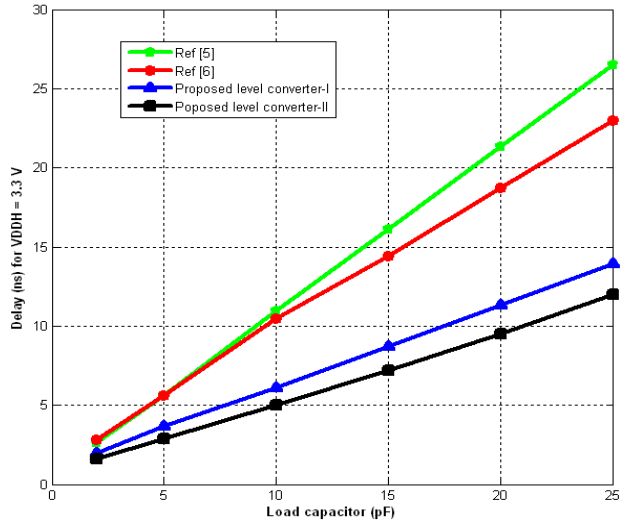

Fig. 20. Proposed level converters and conventional level converters propagation delay comparison for different loading conditions with supply voltage V_{DDH}=3.3 V.

Figure. 21 and 22 represents raise time comparison of proposed level converters and conventional level converters for different loading conditions with supply voltages V_{DDH}=1.8 V and 3.3 V respectively. From Fig. 21 and 22 it is clearly understand that proposed circuit Fig. 7 has less raise times than Fig. 4, 6 and 8. When the load capacitor is increasing raise time of the circuit is increased.

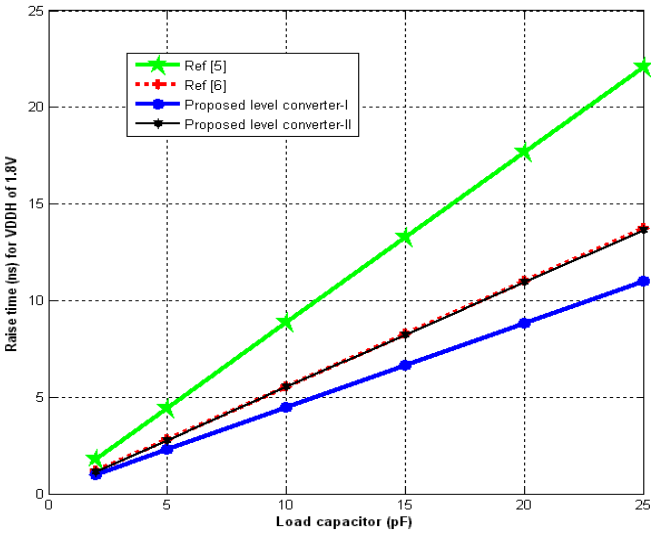

Fig. 21. Proposed level converters and conventional level converters raise time comparison for different loading conditions with supply voltage V_{DDH}=1.8 V.

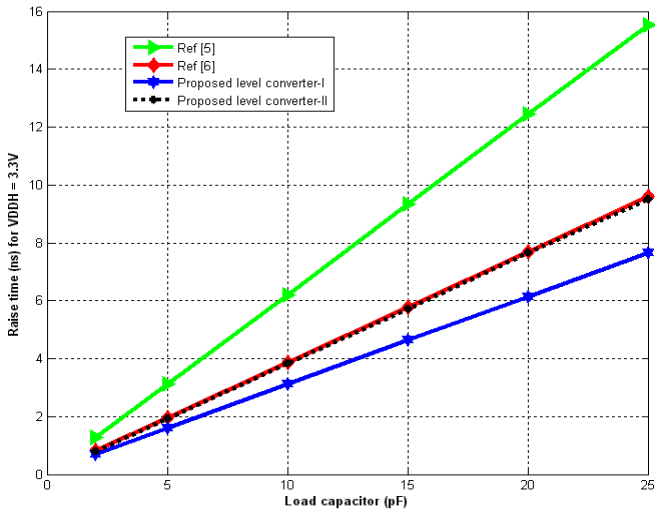

Fig. 22. Proposed level converters and conventional level converters raise time comparison for different loading conditions with supply voltage V_{DDH}=3.3V.

Figure 23 and 24 represents fall time comparison of proposed level converters and conventional level converters for different loading conditions with supply voltages V_{DDH}=1.8 V and 3.3 V respectively. From Fig. 23 and 24 it is clearly understand that proposed circuit Fig. 8 has less raise times than Fig. 4 and 6. When the load capacitor is increasing raise time of the circuit is increased.

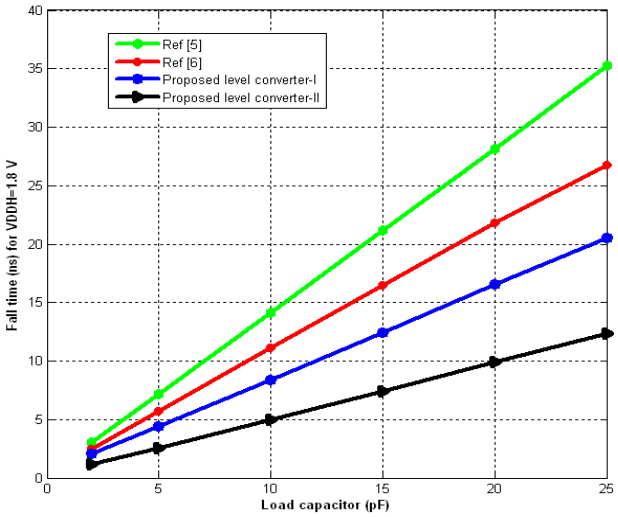

Fig. 23. Proposed level converters and conventional level converters fall time comparison for different loading conditions with V_{DDH}=1.8 V.

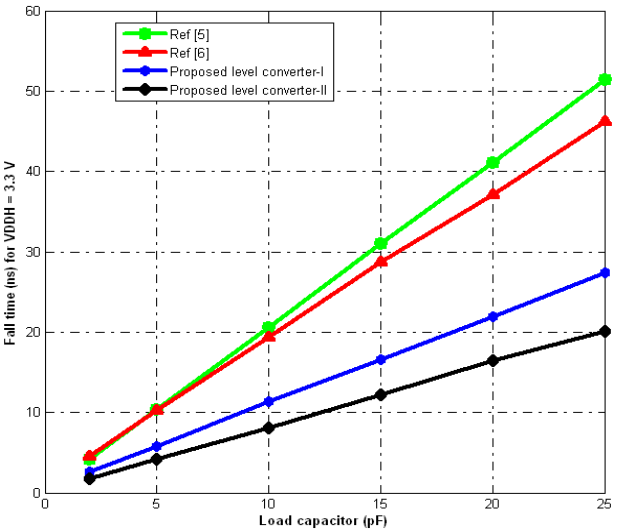

Fig. 24. Proposed level converters and conventional level converters fall time comparison for different loading conditions with supply voltage V_{DDH}=3.3V.

IV. Conclusion

Two Level converters with less delay are proposed using leakage current reduction technique. In leakage current reduction technique used in the existing circuit uses NMOS transistors as resistors by replacing NMOS transistors with PMOS transistors due to higher resistance of PMOS transistors speed performance of proposed circuits is improved. In the existing circuit's diode connected transistors drop a voltage V_{th}, by removing diode connected transistors speed performance of the circuit is further improved with small increase in raise time and decrease in fall time value in proposed level converter-II. Advantage of proposed level converter-I is it has less raise time.

References

[1] A.–J, Annema, B. Nauta, R. Van Langevelde and H. Tuinbout. "Analog circuits in ultra-deep-submicron CMOS", *IEEE Journal of Solid-States Circuits*, vol.40, no.1, DOI: JSSC.2004.837247, 2005, pp.132-143.

[2] D. Pan, Li, H. W. Wilamowski and B.M. "A low voltage to high voltage level shifter circuit For MEMS application", *in Proceedings of the 15th Biennial University/Government/Industry Microelectronics symposium,* DOI: UGIM.2003.1225712, 2003, pp. 128-131.

[3] Bo Zhang, Liping Liang, Xingiun Wang, "A new level shifter with low power in multi voltage system" *In proceedings of 8th International Conference on Solid-State and Integrated Circuit Technology*, DOI:ICSICT.2006.306488, 2006, pp.1857-1859.

[4] S.N. Wooters, B. H. Calhoun, T. N. Blalock, "An Energy-efficient sub threshold level converter in 130nm CMOS", *IEEE Transactions on circuits and systems-II Express Briefs*, Vol. 57, No. 4, DOI:TCSII.2010.2043471 April 2010, pp. 290-294.

[5] H. Shao, C. Y. Tsui. "A robust input voltage adaptive and low energy consumption level converter for sub-threshold logic", *in Proc. of 33rd European Solid-State Circuits Conf. (ESSCIRC)*, DOI:ESSCIRC.2007.4430306, 2007, pp.312-315.

[6] S. Ali, S. Tanner, P. A. Farine. "A robust, low power, high speed voltage level shifter with built-in short circuit current reduction", *in Proc. of 20th European Conf. on Circuit Theory and Design (ECCTD)*, DOI: ECCTD.2011.6043302, 2011, pp.142-145.

[7] I. J. Chang, J. -J. Kim, Roy and K. , "Robust Level Converter Design for Sub-threshold Logic", *in Proc. of the International Symposium on Low Power Electronics and Design (ISLPED)*, DOI:LPE.2006.4271800, 2006, pp.14-19.

[8] M. Vadipour, "A New compensation technique for resistive level shifters" *IEEE Journal of Solid-State Circuits*, vol.28, no.1, 1993, pp.93-95.

[9] Y.Kanno, H.Mizuno, K.Tanaka, T.Watanabe, "Level converters with high immunity to power supply bouncing for high speed sub 1v VLSIs" *In Proceedings of International Symposium on VLSI Circuits Digest of Technical papers*, DOI:VLSIC.2000.852890, 2000, pp.202-203.

[10] Wen-Tai Wang, Ming-Dou Ker, Mi-Chang Chiang, Chung-Hui Chen, "Level shifters for high speed 1V to 3.3V interfaces in a 0.13µm Cu-interconnection/low-k CMOS technology" *In Proceedings of International Symposium on Technical Papers*, DOI: VTSA.2001.934546, 2001, pp.307-310.

[11] Mahendranath. B and Avireni Srinivasulu, "Analysis of two new voltage level converters with various load conditions," International Journal of Advances in Telecommunications, Electrotechnics, Signals and Systems, vol. 2, no. 3, pp. 92-98, 2013. ISSN: 1805-5443.

[12] J.Kim, M. H. Kim, S.L. Kim, C. K. Jeon, Y. S. Choi, H. S. Kang, C. S. Song, "The new high voltage level up shifter for HVIC" *In proceedings of IEEE 33rd Annual Conference on Power Electronics Specialists*, vol.2, DOI: PSEC.2002.1022523, 2002, pp.626-630.

[13] C. Q. Tran, H. Kawaguchi, T. Sakurai, "Low power high speed level shifter design for block level dynamic voltage scaling environment" *In proceedings of International Conference on Integrated Circuit Design and Technology*, DOI:ICICDT.2005.1502637, 2005, pp.229-232.

[14] Won-Ki Park, Cheol-Ung Cha, Sung-Chul Lee, "A Novel level shifter circuit design for display panel drivers" *In Proceedings of 6th IEEE International Midwest Symposium on Circuits and Systems*, vol.2, DOI:MWSCAS.2006.382294, 2006, pp.391-394.

[15] J. F. da Rocha, M.B. dos Santos, J. M. Dores Costa, F. A. Lima, "Level shifter and DCVSL for a low voltage CMOS 4.2V buck converter" *IEEE Transactions on Industrial Electronics*, vol.55, no.9, DOI:TIE.2008.927974, 2008, pp.3315-3323.

[16] J. Rocha, M. Santos, J. M. D. Costa, F. Lima "High voltage tolerant level shifters and DCVSL in standard low voltage CMOS technologies" *In Proceedings of IEEE International Symposium on Industrial Electronics*, DOI: ISIE.2007.4374695, 2007, pp.775-780.

[17] J. C. Garcia, J. A. Montiel-Nelson, S. Nooshaadi, "High performance CMOS dual supply level shifter for a 0.5V input and 1V output in standard 1.2V 65nm technology process" *In proceedings of 9th International Symposium on Communications and Information Technology*, DOI: ISCIT. 2009. 5340988, 2009, pp.963-966.

[18] J. C. Garcia, J. A. Montiel-Nelson, S. Nooshabadi, "High performance bootstrapped CMOS dual supply level shifter for 0.5V input and 1V output" *In Proceedings of 12th Euromicro Conference on Digital System Design, Architectures, Methods and Tools*, DOI: DSD.2009.180, 2009, pp.311-314.

[19] Avireni Srinivasulu and M. Rajesh, "ULPD and CPTL pull-up stages for Differential Cascode Voltage Switch Logic," Journal of Engineering (*Hindawi*), vol. 2013, Article ID 595296, 5 pages, 2013. ISSN: 2314-4912.

[20] D. Wolpert, P. Ampadu, "Level shifter speed, power, and reliability trade-offs across normal and reverse temperature dependences" *In Proceedings of 53rd IEEE International Midwest Symposium on Circuits and Systems,* DOI: MWSCAS.2010.5548766, 2010, pp.1254-1257.

[21] Y. Moghe, T. Lehmann, T. Piessens, "Nanosecond delay floating high voltage level shifters in a 0.35µm HV-CMOS technology" *IEEE Journal of Solid-State Circuits*, vol. 46, no. 2, DOI: JSSC.2010.2091322, 2010, pp.485-497.

Adipudi Bala Tripura Sundari was born in Ongole, Prakasam District, (A.P), India in 1991. She received the B.Tech degree in electronics and communication engineering from J.N.T.University, Kakinada in 2012. She is now working towards her M.Tech thesis in VLSI Design at VFSTR University, Vadlamudi, Guntur, India. Her area of research includes VLSI Design and Microelectronics.

Avireni Srinivasulu was born in Thurimella, Andhra Pradesh, India. He received the B.Tech degree in electronics and communication engineering from Sri Venkateswara University, Tirupati in 1986, M.E, degree in power electronics engineering from Gulbarga University, Gulbarga in 1991, M.S, degree in software systems from Birla Institute of Technology and Science (BITS), Pilani in 1998 and Ph.D, degree in electronics and communication engineering (VLSI Design) from Birla Institute of Technology, Mesra, India in 2010. He is working as a Dean (R&D) and Professor of Electronics and Communication Engineering, VFSTR University, Guntur, India. He has 25 years of teaching and 15 years of research experience in the Department of Electronics and Communication Engineering.

Dr. Avireni.S is a senior member of IEEE, senior member of IACSIT, life member of I.S.T.E and a member of the Institution of Engineers (India). He has published over 50 articles in international journals and international conference proceedings; his main research areas are microelectronics, VLSI design and analog ASIC.

TABLE III. COMPARISON OF SIMULATED PROPAGATION DELAY VALUES OF PROPOSED LEVEL CONVERTERS WITH EXISTING LEVEL CONVERTERS IN DIFFERENT LOAD CONDITIONS.

Level converters	Supply rail voltages		Propagation delay (ns)					
	Input pulse amplitude (V)	V_{DDH}	C_L= 2 pF	C_L =5 pF	C_L =10 pF	C_L =15 pF	C_L =20 pF	C_L =25 pF
Fig. 4 [5]	1	1.8	1.853	3.865	7.229	10.604	13.97	17.33
Fig. 6 [6]	1	1.8	1.75	3.231	5.6895	8.12	10.571	12.84
Proposed level converter-I (Fig. 7)	1	1.8	1.551	2.483	4.154	5.837	7.53	9.216
Proposed level converter-II (Fig. 8)	1	1.8	1.254	2.047	3.4045	4.794	6.144	7.516
Fig. 4 [5]	1	3.3	2.65	5.595	10.95	16.12	21.34	26.537
Fig. 6 [6]	1	3.3	2.84	5.629	10.45	14.42	18.71	22.97
Proposed level converter-I (Fig. 7)	1	3.3	1.981	3.651	6.111	8.71	11.3	13.94
Proposed level converter-II (Fig. 8)	1	3.3	1.633	2.892	5.028	7.169	9.51	11.967

TABLE IV. COMPARISON OF SIMULATED PROPAGATION DELAY, RAISE TIME AND FALL TIME VALUES OF PROPOSED LEVEL CONVERTER-I (FIG. 7)

V_{DDH}	Input pulse amplitude	Capacitor output load C_L								
		5 pF			10 pF			15 pF		
		Raise time(ns)	Fall time(ns)	Propagation delay(ns)	Raise time(ns)	Fall time(ns)	Propagation delay(ns)	Raise time(ns)	Fall time(ns)	Propagation delay(ns)
1.8	0.8	2.327	9	4.893	4.51	17	8.338	6.69	24	11.79
1.8	1	2.3	4.74	2.483	4.47	8.548	4.154	6.645	12.54	5.837
1.8	1.2	2.3	3.413	1.9	4.471	5.947	3.005	6.645	8.577	4.122
3.3	0.8	1.6	11.74	7.203	3.124	22.66	12.66	4.643	33.67	18.18
3.3	1	1.503	5.88	3.651	3.115	11.19	6.111	4.631	16.56	8.71
3.3	1.2	1.59	4.082	2.427	3.113	7.533	4.039	4.63	11.09	5.68

TABLE V. COMPARISON OF SIMULATED PROPAGATION DELAY, RAISE TIME AND FALL TIME VALUES OF PROPOSED LEVEL CONVERTER-II (FIG. 8)

V_{DDH}	Input pulse amplitude	Capacitor output load C_L								
		5 pF			10 pF			15 pF		
		Raise time(ns)	Fall time(ns)	Propagation delay(ns)	Raise time(ns)	Fall time(ns)	Propagation delay(ns)	Raise time(ns)	Fall time(ns)	Propagation delay(ns)
1.8	0.8	2.784	5	3.84	5.505	11	6.46	8.216	16	9.093
1.8	1	2.784	2.597	2.047	5.505	4.967	3.4045	8.216	7.424	4.794
1.8	1.2	2.782	1.681	1.497	5.498	3.233	2.498	8.21	4.77	3.51
3.3	0.8	1.964	8.859	5.77	3.844	16.86	10.23	5.752	25.4	14.77
3.3	1	1.943	4.153	2.892	3.835	8.097	5.028	5.72	12.08	7.169
3.3	1.2	1.943	4.153	2	3.831	5.257	3.341	5.725	7.867	4.775

Chaos Control and Synchronization of Chaotic System Based upon Adaptive Control Algorithm

Israr Ahmad*, Azizan Bin Saaban, Adyda Binti Ibrahim and Mohammad Shahzad

***Abstract*— Controlling chaos is stabilizing one of the unstable periodic orbits either to its equilibrium point or to a stable periodic orbit by means of an appropriate continuous signal injected to the system. On the other hand, chaos synchronization refers to a procedure where two chaotic oscillators (either identical or nonidentical) adjust a given property of their motion to a common behavior. This research paper concerns itself with the Adaptive control and synchronization of a new chaotic system with unknown parameters. Based on the Lyapunov direct method (LDM), the Adaptive control techniques (ACTs) are designed in such a way that the trajectory of the new chaotic system is globally stabilized to one of its equilibrium points of the uncontrolled system. Moreover, the Adaptive control law is also applied to achieve the synchronization state of two identical systems and two different chaotic systems with fully unknown parameters. The parameters identification, chaos control and synchronization of the chaotic system have been carried out simultaneously by the Adaptive controller. All simulation results are carried out to corroborate the effectiveness and the robustness of the proposed methodology and possible feasibility for synchronizing two chaotic systems by using *Mathematica 9*.**

***Keywords*— Chaos Control, Synchronization, Lyapunov Stability Theory, Adaptive Control, Barbalat's Lemma, Chaotic system.**

I. Introduction

Chaotic systems are nonlinear deterministic systems that display a complicated, randomly or disorderly behavior and are very sensitive to its initial condition, i.e. a small perturbation in its initial conditions, the current trajectory of the system may lead to significantly different future behavior [1]. This extreme sensitive effect of the system termed as the "Butterfly effect" [1, 2]. Due to critical dependence upon the initial conditions, it becomes very difficult to make accurate long- term predictions about the system over a given time interval [3]. Despite the complexities of a chaotic attractor, this sensitive dependence upon initial conditions can be exploited to sustain the system about some desired final state by carefully choosing a sequence of small perturbation to a control perimeter or to stabilize an unstable periodic orbit by means of an appropriate continuous signal injected to the system [3, 4]. This is the basic idea behind the so-called the "Control of Chaos"; where one of the infinite number of unstable periodic orbits that naturally embedded in a chaotic attractor is stabilized to either an equilibrium point or to a stable periodic orbit [3].

On the other hand, for the last two decades, another challenging application of chaos research has emerged, which is known as chaos synchronization. Synchronizing chaotic systems is a process where two (or more) chaotic oscillators eventually proceed synonymously for different initial conditions in all future states [5]. This means that the dynamical state of one of the oscillator is completely traced by the dynamical state of the other oscillator. Chaos Synchronization is one of the critical issues and has received a considerable interest among researchers in nonlinear sciences for more than two decades [6, 7] after the exceptional work of Pecorra and Carroll [5]. Until now, certain linear and nonlinear techniques have been proposed and applied successfully to achieve control and synchronization of chaotic systems [8-20]. Notable among those, ACTs is one of the effectual techniques for stabilizing and synchronizing chaotic systems [11-14]. No Lyapunov exponents or gain matrix is required for its execution. These characteristics free the designer to focus on the control and synchronization problems, leaving irksome model manipulations [14].

Most of the traditional control and synchronization techniques [15-17] are utilized when the system parameters are known. However, in practice, the uncertainties, like external disturbances or parameter mismatches, may destroy the chaos control and the synchronization behavior might be disregarded completely. Therefore, it is very important to design a feedback controller and parameter update law for the control and synchronization of chaotic system consisting of unknown parameters. ACT has the advantage of stabilizing and synchronizing chaotic systems with unknown system parameters [11]. ACTs have received considerable attention in the last few years due to its efficiency, robustness and simple in designing [12]. Motivated by the above discussions, the main objectives of this present study can be summarized as follows:

a) Extending the approaches in [11, 12], a simple and efficient ACTs will be designed to stabilize the chaotic system [18] to its unstable equilibrium at the origin with unknown parameters.
b) Based on the Lyapunov Stability Theory (LST) [19]

Manuscript received June 06, 2014, revised September 22, 2014.

Israr Ahmad is with the School of Quantitative Sciences, College of Arts & Sciences, UUM, Saintok Malaysia and with the College of Applied Sciences Nizwa, Ministry of Higher Education, Sultanate of Oman, email: iak_2000plus@yahoo.com

Azizan Bin Saaban and Adyda Binti Ibrahim are with the School of Quantitative Sciences, College of Arts & Sciences, UUM, Saintok Malaysia, emails: azizan.s@uum.edu.my, adyda@uum.edu.my.

Mohammad Shahzad is with the College of Applied Sciences Nizwa, Ministry of Higher Education, Sultanate of Oman, email: dmsinfinite@gmail.com

doi: 10.11601/ijates.v3i2.90

and using the ACTs, a class of appropriate control functions and parameter updated laws will be designed to achieve parameters identification and global chaos synchronization of chaotic system [18].

c) Numerical simulations and graphs will be furnished to show the performance and effectiveness of the proposed schemes.

The rest of the research paper is organized as follows. The problem statement and design of the ACT are presented in section 2. In section 3, the description of the system is given, the new results for stabilizing the uncertain chaotic system [18] are derived, and the ACT is applied to solve the synchronization problem for new chaotic system [18]. In section 4, numerical simulations are carried out to show the efficiency of the proposed approaches and support the analytical results and finally the concluding remarks are then given in section 5.

II. The Problem Statement and Adaptive Feedback Controller Design

A. Problem Statement

Let us consider a chaotic system described as:

$$\dot{x} = g_1(x) + A_1 f_1(x), \quad (1)$$

where $x = [x_1, x_1, ..., x_n]^T$ is the corresponding state vector, $g_1 : R^n \to R^n$ as the nonlinear continuous vector function, $A_1 \in R^m$ is the system parameters vector and $f_1 : R^n \to R^{n\times m}$ is the nonlinear matrix function of system (1).

Let us consider the state function of controlled system (1) to be coupled is given as:

$$\dot{y} = g_2(y) + A_2 f_2(y) + \mu(t), \quad (2)$$

where $y = [y_1, y_1, ..., y_n]^T \in R^{n\times 1}$ is the corresponding state vector, $g_2 \in C^1(R^n, R^n)$ is the nonlinear continuous functions, $A_2 \in R^n$ as the n-dimension parameters vector and $f_2 \in C^1(R^n, R^{n\times k})$ is the nonlinear matrix function of the controlled chaotic system (2) and $\mu(t) \in R^{n\times 1}$ as the feedback controller to the controlled system (2).

As certain stabilization/synchronization algorithms belong to the master-slave systems arrangement. Let us consider the master-slave systems configuration for chaotic system (1) and (2) is described as:

$$\begin{aligned} &\dot{x} = g_1(x) + A_1 f_1(x), && \text{(Master system)} \\ &\dot{y} = g_2(y) + A_2 f_2(y) + \mu(t). && \text{(Slave system)} \end{aligned} \quad (3)$$

By defining the error dynamics as the difference between the master and slave systems (3) given by:

$$\begin{aligned} &e_i(t) = y_i(t) - x_i(t), \ e_i \in R^n, \\ &\dot{e}(t) = g_2(y) + A_2 f(y) - g_1(x) - A_1 f(x) + \mu(t) \Rightarrow \\ &\dot{e}(t) = g_2(y) - g_1(x) + A_2 f(y) - A_1 f(x) + \mu(t) \Rightarrow \\ &\dot{e}(t) = g_2(y) - g_1(x) + A_2 f(y) - A_1 f(x) + \mu(t). \end{aligned} \quad (4)$$

The $F(x, y, e(t)) = g_2(y) - g_1(x)$ is a continuous vector function that contains linear terms and common parts of the master and slave systems.

B. Design of the Adaptive Feedback Controller (ACT)

If $g_1(x) = g_2(y)$, $m = k$ and/or $A_1 = A_2$ then $\boldsymbol{X}$ and $\boldsymbol{Y}$ are the states of two identical (nearly identical) chaotic systems and if, $g_1(x) \neq g_2(y)$, $m \neq k$ and/or $A_1 \neq A_2$, then $\boldsymbol{X}$ and $\boldsymbol{Y}$ are the states of two nonidentical chaotic systems. For the two chaotic systems in the absence of a proper feedback controller, $(\mu_i = 0)$, and for the initial conditions $x_{1m}(0), x_{2m}(0), ..., x_{nm}(0) \neq y_{1s}(0), y_{2s}(0), ..., y_{ns}(0)$, then the trajectories of the two the chaotic systems will quickly diverge from each other in all future states and will become unsynchronized. Hence the basic role of a proper feedback controller '$\mu(t)$' for the chaos control and synchronization problem is such that the error dynamics of (3) converges to zero for all initial conditions, i.e.: $\lim_{t\to\infty} \|e_i(t)\| = \lim_{t\to\infty} \|y_i(t) - x_i(t)\| = 0$ for all $e_i(0) \in R^n$, then the two systems (3) are said to be stabilized/ synchronized. To achieve stabilization/synchronization asymptotically, let us assume the following theorem.

Theorem 1. Trajectories of the two (identical or nonidentical) chaotic oscillators (3) with unknown parameters for all initial conditions $x_{1d}(0), x_{2d}(0), ..., x_{nd}(0) \neq y_{1r}(0), y_{2r}(0), ..., y_{nr}(0)$ will be stabilized/synchronized asymptotically with the fallowing appropriate regular stabilizing nonlinear feedback controller: $\mu(t) = G(x, y) + E(e)$, where $G(x, y)$ are the control variables of $\boldsymbol{X}$ and $\boldsymbol{Y}$, $E(e) = -k_i e_i = -k_i (y_i - x_i)$, $i = 1, 2, ..., n$ is the control function of $e(t)$ and k_i is the coupling strength and a same size with $\mu(t)$.

Proof. Let us consider a positive definite quadratic Lyapunov errors function (PDQLEF) $V(e)$ candidate defined by:

$$V(e) = \frac{1}{2}(ee^T + \bar{A}_1^T \bar{A}_1 + \bar{A}_2^T \bar{A}_2), \quad (5)$$

where $\hat{A}_1$ and $\hat{A}_2$ are the estimated vectors of the unknown parameters and $\bar{A}_1 = A_1 - \hat{A}_1$, $\bar{A}_2 = A_2 - \hat{A}_2$ [10].

It is also assumed that all the variables of the drive and response systems are available and measureable.

It may be noticed that, $V(e) : R^n \to R^n$ is a positive semidefinite function by construction. Now if the time derivative of $V(e)$ along the trajectories of (4) becomes less than or equal to zero (i.e. $\dot{V}(e) \leq 0$ is also a negative semidefinite function); then the errors signal will approach to zero as time tends to infinity and the states of both projected master system and slave system (3) are stabilized/synchronized.

Since $\dot{V}(e) \leq 0$ is a negative semidefinite function and we cannot immediately conclude that the origin is asymptotically stable. To achieve asymptotic stability of the

error dynamics (4), let us introduce the following assumptions and a lemma.

Assumption 1 [20]. The vectors A_1, A_2 of the unknown positive parameters are always bounded.

Assumption 2 [21]. If $e_1, e_2, ..., e_n \in L^2 \cap L^\infty < \infty$ and $\dot{e}_1, \dot{e}_2, ..., \dot{e}_n \in L^2 < \infty$, then $e(t) = [e_1(t), e_2(t), ..., e_n(t)]$ is also bounded.

Lemma [22]. Let for a non-increasing function $V(t) \in C^1$, $\dot{V}(e)$ is uniformly continuous, negative semidefinite and radially unbounded function with: $V(0) = 0$, $V(t) > 0$ for all $t \neq 0$ and $\|t\| \to \infty \Rightarrow V(t) \to \infty$ then $\lim_{t\to\infty} \dot{V}(e) = 0$.

III. New Chaotic System Description

A. Description of New Chaotic System

Recently, Chunlai Li, *et al* [18] have proposed and studied a 3-D autonomous chaotic system on the same construction patterns of Chen, Liu and Qi chaotic systems. Chunlai Li, et.al, have added a quadratic nonlinear term to the first equation of Chen system and proposed a new 3-D chaotic system which is topologically different and have more complex dynamic than those of Chen, Liu and Qi Chaotic Systems. The new system can produce a typical double-wing chaotic attractor. The differential equations describing the dynamics of the considered chaotic system are given as:

$$\begin{aligned} \dot{x} &= p(y - x) + yz, \\ \dot{y} &= (r - p)x + ry - xz, \\ \dot{z} &= -qz + sy^2, \end{aligned} \tag{6}$$

where $x, y, z \in R^n$ are the state variables and *p*, *q*, *r* and *s* are the unknown real parameters of the system. By linearizing the system (6) at the equilibrium point $E_0 = (0,0,0)$ for the parameters values *p*, *q*, *r* and *s*. The Jacobean matrix is given as:

$$J_{(0,0,0)} = \begin{bmatrix} -p & p & 0 \\ (r-p) & r & 0 \\ 0 & 0 & -q \end{bmatrix}.$$

The characteristic equation of $J_{(0,0,0)}$ is given as:

$$\lambda^3 + (p + q - r)\lambda^2 + (p^2 + pq - rq - 2pr)\lambda + \\ + p^2 q - 2pqr = 0.$$

For the parameters values $p = 40, q = 5, r = 30$ and $s \in [0,10]$ the three eigenvalues are $\lambda_1 = -33.7225$, $\lambda_2 = -5$ and $\lambda_3 = 23.7228$.

In continuous nonlinear dynamical systems, the condition for stability is that all the eigenvalues and Lyapunov exponents must be negative. We can see that the two eigenvalues are negative and one eigenvalue is positive ($\lambda_1, \lambda_2 < 0$ and $\lambda_3 > 0$) with the Lyapunov exponents $L_1 = 3.88$, $L_2 = 0.00$, $L_3 = -25.52$ [18] respectively, which confirm that the system (7) is globally unstable at the equilibrium point $E_0 = (0,0,0)$. On any initial condition on one of the negative eigenvector, the orbit will converges to the equilibrium point $E_0 = (0,0,0)$ through the eigen plane of these two negative eigenvectors but any deviation along $\lambda_3 > 0$ will expand and the orbit becomes unstable which shows a saddle point. Hence from the Lyapunov Stability Theory (LST) [19], the equilibrium point $E_0 = (0,0,0)$ is unstable. Physically, this result bears the fact that the system can oscillate chaotically and prohibits the existence of stable fixed point motion in the system. Thus the new system [18] exhibits a chaotic attractor for parameters values $p = 40$, $q = 5$, $r = 30$ and $s \in [0,10]$ and hence the control problem takes place.

For the dynamical properties such as the equilibrium points, the maximum Lyapunov exponents' spectrum analysis, the phase portraits and the bifurcation diagram etc for the system (6), one may refer to [18].

B. Tracking Problem for New Chaotic System

The main objective of this section is to stabilize the new chaotic system to its equilibrium point at the origin by using the ACT when the parameters of the system [18] are fully unknown. Therefore, let us consider the controlled chaotic system (6) described as:

$$\begin{aligned} \dot{x} &= p(y - x) + yz + \mu_1, \\ \dot{y} &= (r - p)x + ry - xz + \mu_2, \\ \dot{z} &= -qz + sy^2 + \mu_3, \end{aligned} \tag{7}$$

where $x, y, z \in R^n$ are the state variables of the system and $\mu(t) = [\mu_1(t), \mu_2(t), \mu_3(t)]^T$ as the stabilizing feedback controller that yet to be designed using the states and estimates of unknown parameters of the uncertain chaotic system.

In the absence of a proper feedback controller, ($\mu_i(t) = 0$),if the initial conditions are $x_{i1}(0), x_{i2}(0), ..., x_{in}(0) \neq y_{j1}(0), y_{j2}(0), ..., y_{jn}(0)$ then the trajectories of the chaotic system will quickly bifurcate from each other in all future states and the system will become unstable. Hence, the role of a proper feedback controller for the chaos stabilization problem is to restrict the system converges to $E_0 = (0,0,0)$ for all initial conditions, then the chaotic system is said to be stabilized at the equilibrium point. Thus the main focus of this part is to stabilize the chaotic system (6) at the origin asymptotically by determining a proper AFC. In order to achieve the global chaos stabilization of system (6), let us assume the following theorem.

Theorem 2. The trajectories of the chaotic oscillator (7) with unknown parameters for all initial conditions ($x_{i1}(0), y_{i2}(0), z_{i3}(0) \neq x_{j1}(0), y_{j2}(0), z_{j3}(0)$)will be stabilized asymptotically with the following appropriate regular stabilizing AFC [12] and parameter estimation law given in (15):

$$\begin{aligned}\mu_1(t) &= -\hat{p}(y-x) - yz - k_1 x,\\ \mu_2(t) &= -(\hat{r}-\hat{p})x - \hat{r}y + xz - k_2 y,\\ \mu_3(t) &= -\hat{q}z + \hat{s}y^2 + k_3 z,\end{aligned} \tag{8}$$

where $\hat{p}$, $\hat{q}$, $\hat{r}$ and $\hat{s}$ are the estimated value of the unknown parameters *p*, *q*, *r* and *s* respectively and k_i $(i = 1, 2, 3)$ are the feedback gains.

Proof. Replacing system of equations (8) in (7), we get:

$$\begin{aligned}\dot{x} &= (p-\hat{p})(y-x) - k_1 x,\\ \dot{y} &= (r-\hat{r})x - (p-\hat{p})x + (r-\hat{r})y - k_2 y,\\ \dot{z} &= -(q-\hat{q})z + (s-\hat{s})y^2 - k_3 z.\end{aligned} \tag{9}$$

Let us define the parameter estimation errors as:

$$e_p = p-\hat{p},\ e_r = r-\hat{r},\ e_q = q-\hat{q},\ e_s = s-\hat{s}, \tag{10}$$

$$\dot{e}_p = -\dot{\hat{p}},\ \dot{e}_r = -\dot{\hat{r}},\ \dot{e}_q = -\dot{\hat{q}},\ \dot{e}_s = -\dot{\hat{s}}. \tag{11}$$

Replacing equation (10) in (9), the closed-loop dynamics becomes:

$$\begin{aligned}\dot{x} &= e_p(y-x) - k_1 x,\\ \dot{y} &= \left(e_r - e_p\right)x + e_r y - k_2 y,\\ \dot{z} &= -e_q z + e_s y^2 - k_3 z.\end{aligned} \tag{12}$$

For determination of the updated law for adjusting the estimation of the parameters, Let us construct a PDQLEF candidate [12] *V*(*e*) defined by:

$$V(e) = \frac{1}{2}(x^2 + y^2 + z^2 + {e_p}^2 + {e_r}^2 + {e_q}^2 + {e_s}^2) \geq 0, \tag{13}$$

Now the time derivative of the Lyapunov error function (LEF) along the trajectory of the closed loop system (12) is given as:

$$\begin{aligned}\dot{V}(e) &= (x\dot{x} + y\dot{y} + z\dot{z} + e_p\dot{e}_p + e_r\dot{e}_r + e_q\dot{e}_q + e_s\dot{e}_s),\\ \dot{V}(t) &= -k_1x^2 - k_2y^2 - k_3z^2 + e_p\left((y-x)x - xy - \dot{\hat{p}}\right) +\\ &+ e_r\left((x+y)y - \dot{\hat{r}}\right) + e_q\left(-z^2 - \dot{\hat{q}}\right) + e_s\left(y^2 z - \dot{\hat{s}}\right),\end{aligned} \tag{14}$$

Let us estimate the parameters $\hat{p}$, $\hat{q}$, $\hat{r}$ and $\hat{s}$ by the following update law:

$$\begin{aligned}&\dot{\hat{p}} = (y-x)x - xy + k_4 e_p,\ \dot{\hat{r}} = (x+y)y + k_5 e_r,\\ &\dot{\hat{q}} = -z^2 + k_6 e_q,\ \dot{\hat{s}} = y^2 z + k_7 e_s.\end{aligned} \tag{15}$$

Therefore using (15) $\dot{V}(e) = -k_1x^2 - k_2y^2 - k_3z^2 - k_4{e_p}^2 -$ $-k_5{e_r}^2 - k_6{e_q}^2 - k_7{e_s}^2 \leq 0$, which is a negative semidefinite function on R^7 if $k_i \leq 0$ for $i = 1, 2., .., 7$. Hence the error dynamics is asymptotically stable at the origin.

C. Identical Synchronization of new Chaotic System with Parameters Estimation

Most of the synchronization algorithms belong to the master-slave system arrangement. By master-slave system arrangement means that the two chaotic oscillators are coupled in such a way in which one chaotic oscillator is forced to track the other oscillator and the states of two chaotic oscillators show uniform behavior. In order to observe the identical synchronization for chaotic system (6), let us consider the master-slave systems arrangement is described as:

$$\begin{aligned}\dot{x}_1 &= p(y_1 - x_1) + y_1 z_1,\\ \dot{y}_1 &= (r-p)x_1 - x_1 z_1 + r y_1, \text{ (Master System)}\\ \dot{z}_1 &= -q z_1 + s{y_1}^2,\end{aligned} \tag{16}$$

and

$$\begin{aligned}\dot{x}_2 &= p(y_2 - x_2) + \eta_1,\\ \dot{y}_2 &= (r-p)x_2 - x_2 z_2 + r y_2 + \eta_2, \text{ (Slave System)}\\ \dot{z}_2 &= -q z_2 + s{y_2}^2 + \eta_3,\end{aligned} \tag{17}$$

where $x_1, y_1, z_1 \in R^n$ and $x_2, y_2, z_2 \in R^n$ are the state variables and *p*, *q*, *r* and *s* of the master and slave systems respectively and $\eta(t) = [\eta_1(t), \eta_2(t), \eta_3(t)]^T \in R^{3\times 1}$ as the stabilizing nonlinear feedback control function introduced to the slave system that is yet to be designed. By defining the synchronization error dynamics as the difference between the master and slave systems given by $e_i(t) = y_i(t) - x_i(t),\ e_i(t) \in R^n$ for $i = 1, 2, 3$.

Thus the time varying error dynamics for the master (15) and slave (16) systems yields as:

$$\begin{aligned}\dot{e}_1 &= p(e_2 - e_1) + y_2 z_2 - y_1 z_1 + \eta_1,\\ \dot{e}_2 &= (r-p)e_1 + r e_2 + (x_1 z_1 - x_2 z_2) + \eta_2,\\ \dot{e}_3 &= -q e_3 + s({y^2}_2 - {y^2}_1) + \eta_3.\end{aligned} \tag{18}$$

The aim of the synchronization problem is to design a feedback controller '$\eta(t)$' so that the difference between the trajectories of the two coupled chaotic systems (16) and (17) becomes zero for all future states in the course of time, i.e. $\lim_{t\to\infty}\|e(t)\| = 0$, where $e(t) = [e_1(t), e_2(t), e_3(t)]^T$.

The main focus of this section is to investigate and study the synchronization problem of two identical chaotic systems (16) and (17) with fully unknown parameters. It is clear that the synchronization of two chaotic systems is equivalent to the problem of stabilizing the system (14) at the equilibrium point (0,0) by determining a suitable feedback controller '$\eta(t)$' and parameter estimation and proper updated laws for system of equations (18) so that when synchronizing the two chaotic systems (16) and (17), the effect of nonlinearity of chaotic systems does not neglect and the error dynamics (18) of the two identical chaotic systems (16) and (17) converges to the equilibrium point asymptotically with less control effort and sufficient transient speed. For these motivations, we assume the following theorem.

Theorem 3. The trajectories of the two identical chaotic systems (16) and (17) for all initial conditions $\left(x_{1m}(0), x_{2m}(0), x_{3d}(0) \neq y_{1s}(0), y_{2s}(0), y_{3s}(0)\right)$ will be synchronized asymptotically with fully unknown parameters by the fallowing appropriate regular stabilizing AFC functions and parameter estimation law given in (26) as:

$$\eta_1(t) = -\hat{p}(e_2 - e_1) + y_1 z_1 - y_2 z_2 - k_1 e_1,$$
$$\eta_2(t) = -(\hat{r} - \hat{p})e_1 + x_2 z_2 - x_1 z_1 - \hat{r} e_2 - k_2 e_2, \quad (19)$$
$$\eta_3(t) = \hat{q} e_3 - \hat{s}(y^2{}_2 - y^2{}_1) - k_3 e_3,$$

where $\hat{p}$, $\hat{q}$, $\hat{r}$ and $\hat{s}$ are the estimated value of the unknown parameters *p*, *q*, *r* and *s* respectively and k_i are the control gains.

Proof. Replacing system of equation (19) in (18), we get:

$$\dot{e}_1 = (p - \hat{p})(e_2 - e_1) - k_1 e_1,$$
$$\dot{e}_2 = (r - \hat{r})e_1 - (p - \hat{p})e_1 + (r - \hat{r})e_2 - k_2 e_2, \quad (20)$$
$$\dot{e}_3 = -(q - \hat{q})e_3 + (s - \hat{s})(y^2{}_2 - y^2{}_1) - k_3 e_3.$$

Let us define the parameter estimation errors as:

$$e_p = p - \hat{p},\ e_r = r - \hat{r},\ e_q = q - \hat{q},\ e_s = s - \hat{s}, \quad (21)$$

$$\dot{e}_p = -\dot{\hat{p}},\ \dot{e}_r = -\dot{\hat{r}},\ \dot{e}_q = -\dot{\hat{q}},\ \dot{e}_s = -\dot{\hat{s}}. \quad (22)$$

Substituting equation (21) in (20), the error dynamics can be described as:

$$\dot{e}_1 = e_p(e_2 - e_1) - k_1 e_1,$$
$$\dot{e}_2 = (e_r - e_p)e_1 + e_r e_2 - k_2 e_2, \quad (23)$$
$$\dot{e}_3 = -e_q e_3 + e_s(y^2{}_2 - y^2{}_1) - k_3 e_3,$$

For determination of the updated law for adjusting the estimation of the parameters, let us construct the same PDQLEF candidate as in (13):

$$V(e) = \frac{1}{2}\sum_{i=1}^{3}(e_i{}^T e_i) + \frac{1}{2}(e_p{}^2 + e_r{}^2 + e_q{}^2 + e_s{}^2) \geq 0. \quad (24)$$

Now the time derivative of the LEF along the direction of the error dynamics (23) as:

$$\dot{V}(e) = (e_1\dot{e}_1 + e_2\dot{e}_2 + e_3\dot{e}_3 + e_p\dot{e}_p + e_r\dot{e}_r + e_q\dot{e}_q + e_s\dot{e}_s),$$
$$\dot{V}(e) = -k_1 e_1{}^2 - k_2 e_2{}^2 - k_3 e_3{}^2 - e_p\left(e_1{}^2 + \dot{\hat{p}}\right) -$$
$$-e_r\left(-e_2(e_1 + e_2) + \dot{\hat{r}}\right) - e_q\left(e_3{}^2 + \dot{\hat{q}}\right) - \quad (25)$$
$$-e_s\left(-e_3(y_2{}^2 - y_1{}^2) + \dot{\hat{s}}\right).$$

When the master system's parameters are not available, then we can achieve parameters identification and synchronization simultaneously with the controlled slave system and the parameters estimation update law. Based on (25), the update laws $\hat{p}$, $\hat{q}$, $\hat{r}$ and $\hat{s}$ for the parameters estimates is derived according to the following update law:

$$\dot{\hat{p}} = -e_1{}^2 + k_4 e_p,\ \dot{\hat{r}} = (e_1 + e_2)e_2 + k_5 e_r,$$
$$\dot{\hat{q}} = -e_3{}^2 + k_6 e_q,\ \dot{\hat{s}} = (y_2{}^2 - y_1{}^2)e_3 + k_7 e_s. \quad (26)$$

With this choice of controller (19) and the parameters estimation update laws (26) yields:

$$\dot{V}(e) = -\left[\left(\sum_{i-1}^{3} k_i e_i{}^2\right) + \left(e_p{}^2 + e_q{}^2 + e_r{}^2 + e_s{}^2\right)\right] \leq 0, \quad (27)$$

i.e. $\dot{V}(e) = -e^T P e \leq 0$, Which is a negative semidefinite function on R^7 [14]. Hence the error dynamics is stable at the origin.

Since from (24) and (27), a_1, b_1, c_1, d_1, δ_1, f_1 and g_1 are bounded [20], as $e_1, e_2, e_3 \in L^2 \cap L^\infty < \infty$ and $\dot{e}_1, \dot{e}_2, \dot{e}_3 \in L^2 < \infty$. It can be easily check that $\ddot{e}(t)$ is bounded. Thus from (20) $\left[e_1(t), e_2(t), e_3(t)\right]$ is also bounded [21]. As the trajectories of chaotic systems are always bounded [23], so from (19), $\eta(t)$ is also bounded. Therefore, if $\lambda_{\min}(P)$ is the minimum eigenvalue of a positive definite matrix P, then by Barbalat's lemma [22]:

$$\int_0^t \lambda_{\min}(P)\|e\|^2 dt \leq \int_0^t (e^T P e)dt = \int_0^t -\dot{V}(t)dt = V(0) - V(t) \leq 0.$$

This implies that, $\lim_{t\to\infty}\|e_i(t)\| = 0$, for $i = 1, 2, 3$.

Hence the equilibrium point (origin) is asymptotically stable. Thus by the LST [19], it is evident that the synchronization errors and parameter estimation errors are decay to zero asymptotically with the course of time for all initial conditions. Hence the two coupled chaotic systems (16) and (17) with unknown parameters are asymptotically synchronized.

D. Chaos Synchronization of Nonidentical Chaotic Systems with Parameters Estimation

In order to observe the switching synchronization for chaotic system (5), it is assumed that the new chaotic system drives the Liu chaotic system [24]. Therefore the master is described as:

$$\dot{x}_1 = p(y_1 - x_1) + y_1 z_1,$$
$$\dot{y}_1 = (r - p)x_1 + r y_1 - x_1 z_1, \text{ (Master system)} \quad (27)$$
$$\dot{z}_1 = -q z_1 + s y_1{}^2,$$

and the slave system, we consider the controlled Liu chaotic system as:

$$\dot{x}_2 = \alpha(y_2 - x_2) + \eta_1,$$
$$\dot{y}_2 = \beta x_2 - x_2 z_2 + \eta_2, \text{ (Slave system)} \quad (28)$$
$$\dot{z}_2 = -\gamma z_2 + \delta x_2{}^2 + \eta_3,$$

where $x_1, y_1, z_1 \in R^n$ and $x_2, y_2, z_2 \in R^n$ are the corresponding state vectors of master and slave systems respectively, *p*, *q*, *r* and *s* are the system parameters of the master system and α, β, γ and δ are the system parameters of the slave system respectively and $\eta(t) = [\eta_1(t), \eta_2(t), \eta_3(t)]^T \in R^{n\times 1}$ as the AFC that yet to be designed. The error dynamics for the master (27) and slave (28) systems can be described as:

$$\dot{e}_1 = \alpha(y_2 - x_2) - p(y_1 - x_1) - y_1 z_1 + \eta_1,$$
$$\dot{e}_2 = \beta x_2 - (r - p)x_1 - r y_1 + x_1 z_1 - x_2 z_2 + \eta_2, \quad (29)$$
$$\dot{e}_3 = -\gamma z_2 + q z_1 + \delta x_2{}^2 - s y_1{}^2 + \eta_3.$$

The main contribution of this section is to achieve asymptotic synchronization between two different chaotic systems (27) and (28) with fully unknown parameters such that the synchronization errors and parameter estimation errors are decay to zero with the course of time for all initial

conditions: $(x_{1d}(0), x_{2d}(0), ..., x_{nd}(0) \neq y_{1r}(0), y_{2r}(0), ..., y_{nr}(0))$; by designing such a feedback adaptive controller that the Liu system [24] force to track the new system [18] and the two systems show similar behavior for all future states. To achieve these objectives, let us assume the following theorem.

Theorem 4. The trajectories of the two nonidentical chaotic systems (27) and (28) for all initial conditions $(x_{1m}(0), x_{2m}(0), x_{3d}(0) \neq y_{1s}(0), y_{2s}(0), y_{3s}(0))$ will be synchronized asymptotically with fully unknown parameters by the fallowing appropriate regular stabilizing AFC functions and parameter estimation law given in (37) as:

$$\begin{aligned}
\eta_1(t) &= -\hat{\alpha}(y_2 - x_2) + \hat{p}(y_1 - x_1) + y_1 z_1 - k_1 e_1, \\
\eta_2(t) &= -\hat{\beta} x_2 + (\hat{r} - \hat{p}) x_1 + \hat{r} y_1 + x_2 z_2 - x_1 z_1 - k_2 e_2, \\
\eta_3(t) &= \hat{\gamma} z_2 - \hat{q} z_1 - \hat{\delta} x_2^{\,2} + \hat{s} y_1^{\,2} - k_3 e_3,
\end{aligned} \tag{30}$$

where $\hat{p}$, $\hat{q}$, $\hat{r}$ and $\hat{s}$, and $\hat{\alpha}$, $\hat{\beta}$, $\hat{\gamma}$ and $\hat{\delta}$ are the estimated value of the unknown parameters *p, q, r* and *s*, and α, β, γ and δ respectively and k_i are the feedback gains.

Proof. Replacing system of equations (30) in (29), the error dynamics can be expressed as:

$$\begin{aligned}
\dot{e}_1 &= (\alpha - \hat{\alpha})(y_2 - x_2) - (p - \hat{p})(y_1 - x_1) - k_1 e_1, \\
\dot{e}_2 &= (\beta - \hat{\beta}) x_2 - (r - \hat{r}) x_1 + (p - \hat{p}) x_1 - (r - \hat{r}) y_1 - k_2 e_2, \\
\dot{e}_3 &= -(\gamma - \hat{\gamma}) z_2 + (q - \hat{q}) z_1 + (\delta - \hat{\delta}) x_2^{\,2} - (s - \hat{s}) y_1^{\,2} - k_3 e_3.
\end{aligned} \tag{31}$$

Let us define the parameter estimation errors as:

$$\begin{aligned}
e_p &= p - \hat{p}, e_r = r - \hat{r}, e_q = q - \hat{q}, e_s = s - \hat{s}, \\
e_\alpha &= \alpha - \hat{\alpha}, e_\beta = \beta - \hat{\beta}, e_\gamma = \gamma - \hat{\gamma}, e_\delta = \delta - \hat{\delta},
\end{aligned} \tag{32}$$

$$\begin{aligned}
\dot{e}_p &= -\dot{\hat{p}}, \dot{e}_r = -\dot{\hat{r}}, \dot{e}_q = -\dot{\hat{q}}, \dot{e}_s = -\dot{\hat{s}}, \\
\dot{e}_\alpha &= -\dot{\hat{\alpha}}, \dot{e}_\beta = -\dot{\hat{\beta}}, \dot{e}_\gamma = -\dot{\hat{\gamma}}, \dot{e}_\delta = -\dot{\hat{\delta}}.
\end{aligned} \tag{33}$$

Replacing system of equation (31) in (32), the error dynamics can be described as:

$$\begin{aligned}
\dot{e}_1 &= e_\alpha (y_2 - x_2) - e_p (y_1 - x_1) - k_1 e_1, \\
\dot{e}_2 &= e_\beta x_2 - e_r x_1 + e_p x_1 - e_r y_1 - k_2 e_2, \\
\dot{e}_3 &= -e_\gamma z_2 + e_q z_1 + e_\delta x_2^{\,2} - e_s y_1^{\,2} - k_3 e_3.
\end{aligned} \tag{34}$$

For determination of the updated law for adjusting the estimation of the parameters, let us construct PDQLEF candidate as in (13):

$$\begin{aligned}
V(e) = \frac{1}{2}\sum_{i=1}^{3}(e_i^{\,T} e) + \frac{1}{2}(e_p^{\,2} + e_r^{\,2} + e_q^{\,2} + e_s^{\,2} + e_\alpha^{\,2} + \\
+ e_\beta^{\,2} + e_\gamma^{\,2} + e_\delta^{\,2}) \geq 0,
\end{aligned} \tag{35}$$

which is a positive definite function on R^{11}.

Now the time derivative of the LEF along the trajectories of the error dynamics (34) as:

$$\begin{aligned}
\dot{V}(e) = &-k_1 e_1^{\,2} - k_2 e_2^{\,2} - k_3 e_3^{\,2} - e_p\left((y_1 - x_1)e_1 - e_2 x_1 + \dot{\hat{p}}\right) + \\
&+ e_q\left(e_3 z_1 - \dot{\hat{q}}\right) - e_r\left((x_1 + y_1)e_2 + \dot{\hat{r}}\right) - e_s\left(e_3 y_1^{\,2} + \dot{\hat{s}}\right) + \\
&+ e_\alpha\left((y_2 - x_2)e_1 - \dot{\hat{\alpha}}\right) + e_\beta\left(e_2 x_2 - \dot{\hat{\beta}}\right) \\
&- e_\gamma\left(e_3 z_2 + \dot{\hat{\gamma}}\right) + e_\delta\left(e_3 x_2^{\,2} - \dot{\hat{\delta}}\right).
\end{aligned} \tag{36}$$

When the master system's parameters are not available, then we can achieve parameters identification and synchronization simultaneously with the controlled slave system and the parameters estimation update law. Based on (36), the update laws $\hat{p}$, $\hat{q}$, $\hat{r}$, $\hat{s}$, $\hat{\alpha}$, $\hat{\beta}$, $\hat{\gamma}$ and $\hat{\delta}$ for the parameters estimates are derived according to the following update law:

$$\begin{aligned}
&\dot{\hat{p}} = -(y_1 - x_1)e_1 + e_2 x_1 + k_4 e_p, \\
&\dot{\hat{q}} = e_3 z_1 + k_5 e_q, \dot{\hat{r}} = -(x_1 + y_1)e_2 + k_6 e_r, \\
&\dot{\hat{s}} = -e_3 y_1^{\,2} + k_7 e_s, \\
&\dot{\hat{\alpha}} = (y_2 - x_2)e_1 + k_8 e_\alpha, \dot{\hat{\beta}} = e_2 x_2 + k_9 e_\beta, \\
&\dot{\hat{\gamma}} = -e_3 z_2 + k_{10} e_\gamma, \dot{\hat{\delta}} = e_3 x_2^{\,2} + k_{11} e_\delta.
\end{aligned} \tag{37}$$

With this choice of controller (30) and the updated laws (37), the LEF (36) yields:

$$\begin{aligned}
\dot{V}(e) = -\sum_{i=1}^{3}(k_i e_i^{\,2}) - (k_4 e_p^{\,2} + k_5 e_r^{\,2} + k_6 e_q^{\,2} + \\
+ k_7 e_s^{\,2} + k_8 e_\alpha^{\,2} + k_9 e_\beta^{\,2} + k_{10} e_\gamma^{\,2} + k_{11} e_\delta^{\,2}) \leq 0,
\end{aligned}$$

i.e. $\dot{V}(e) = -e^T P e \leq 0$, Which is a negative semidefinite function on R^{11} and $P = \begin{pmatrix} k_1 & 0 & . & . & 0 \\ 0 & k_2 & 0 & . & 0 \\ . & . & . & . & . \\ . & . & . & . & . \\ 0 & 0 & . & . & k_{11} \end{pmatrix}$. Hence the error dynamics (34) is stable. Using assumption 1 & 2, $[e_1(t), e_2(t), e_3(t)]$ and $\eta(t)$ are bounded. Therefore, if $\lambda_{\min}(P)$ is the minimum eigenvalue of a positive definite matrix P, then by Barbalat's lemma [21]:

$$\int_0^t \lambda_{\min}(P)\|e\|^2 dt \leq \int_0^t (e^T P e)\, dt = \int_0^t -\dot{V}(t) dt = V(0) - V(t) \leq 0 \cdot$$

Thus, the error dynamics (34) converges to equilibrium point asymptotically, i.e. $\lim_{t\to\infty}\|e_i(t)\| = 0$ for $i = 1, 2, 3$. Hence based on the LST [19], it is obvious that the synchronization errors and parameter estimation errors are decay to zero asymptotically with the course of time for all initial conditions: $(x_{i1}(0), y_{i2}(0), z_{i3}(0) \neq x_{j1}(0), y_{j2}(0), z_{j3}(0))$. Thus the two nonidentical chaotic systems (27) and (28) with fully unknown parameters are asymptotically synchronized.

IV. Numerical Simulations and Discussion

The numerical simulations were carried out using the *Mathematica* 9. For this numerical simulation, the parameters for the new chaotic system [18] are selected as: $p=40$, $q=5$, $r=30$, $s=3$, with initial conditions: (2, -3, 2) and (-5, -7, 5). The four unknown parameters are taken in simulations so that the new system [18] exhibit chaotic attractor.

For the adaptive and update law, the feedback control gains are taken as: $k_i=3$ for $i=1,2,....,11$. The parameters for the Liu chaotic system [24] are taken as: $\alpha=10$, $\beta=40$, $\gamma=2.5$, $\delta=4$, with initial values: (8, 21, 17) and (15, 7, 6).

For the chaotic system [18] the time histories of the state vectors of controlled and uncontrolled are provided in Figs. 1 to 3, which shows the system [18] is well controlled after transient time of 0.2 s; which justified the performance of using the type of control schemes presented in this research work. Figure 4 illustrates the time history of the parameters estimates for suppressing chaos in the new system under the update law (14) and Fig. 9 and 14 shows the time history of the parameters estimates for synchronizing the system [18] with the initial estimated parameters $p_1(0)=22$, $q_1(0)=10$, $r_1(0)=36$ and $s_1(0)=6$. It is clear that the estimations $\hat{p}$, $\hat{q}$, $\hat{r}$ and $\hat{s}$ of unknown parameters *p*, *q*, *r*, and *s* converge to *p*, *q*, *r*, and *s* respectively as time goes to infinity under the update laws (26) and (37).

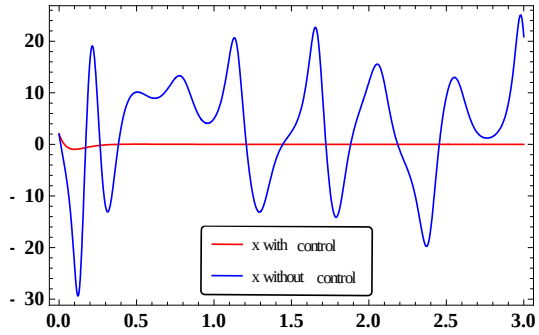

Figure 1: Time Series of x

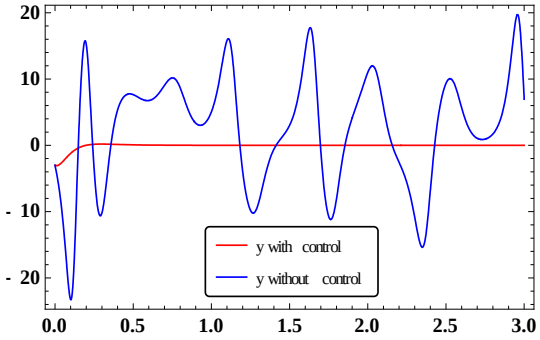

Figure 2: Time Series of y

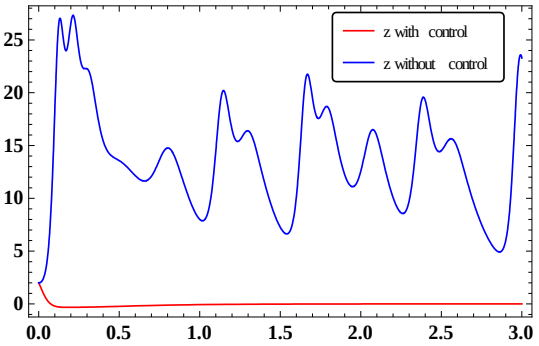

Figure 3: Time Series of z

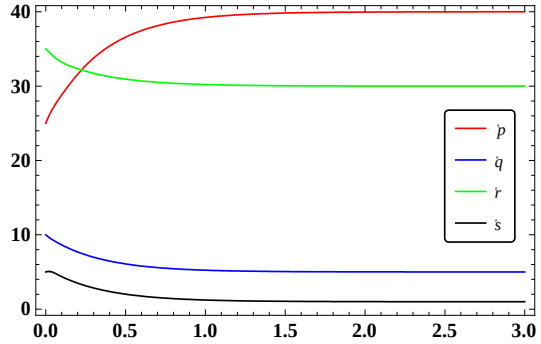

Figure 4: Time Series of update vectors For stabilization

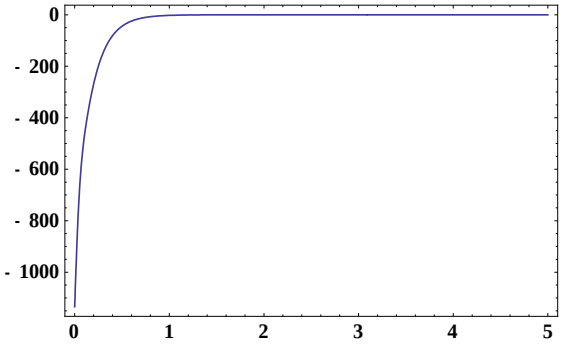

Figure 5: Time Series of $\dot{V}(t)$ for chaos stabilization

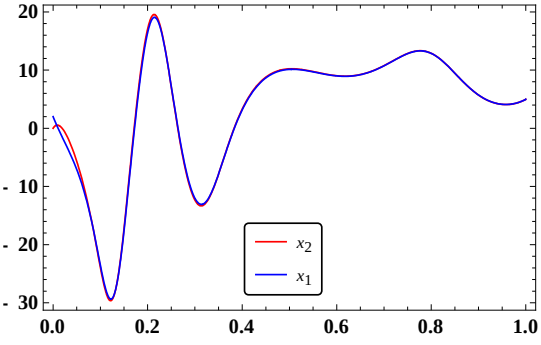

Figure 6: Time Series of x_2 & x_1 for identical synchronization

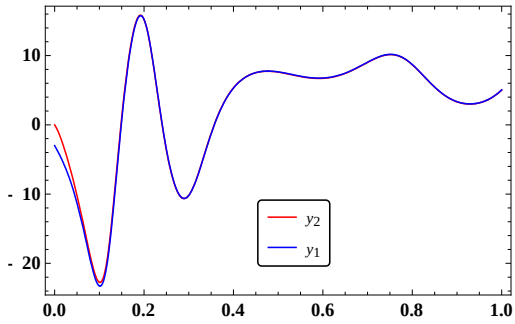

Figure 7: Time Series of y_2 & y_1 for identical synchronizatior

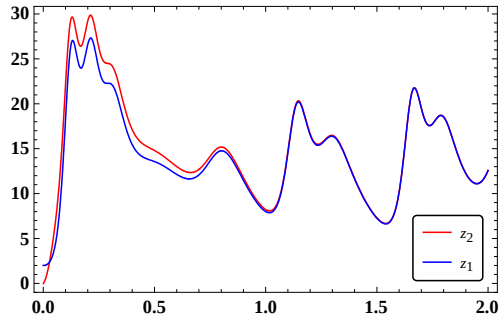

Figure 8: Time Series of z_2 & z_1 for identical synchronizatior

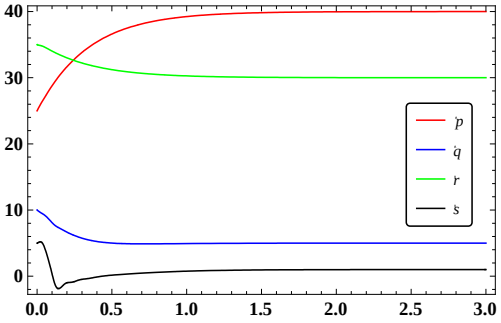

Figure 9: Time Series of $\dot{p}, \dot{q}, \dot{r}$ & $\dot{s}$ for identical synchronizatior

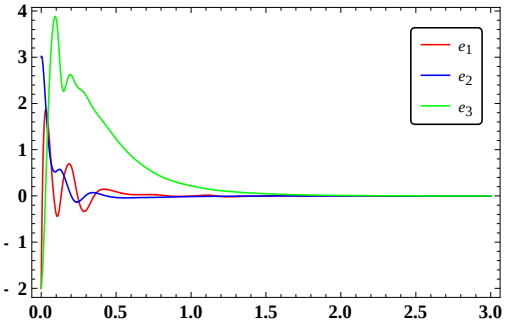

Figure 10: Time Series of errors for identical synchronizatior

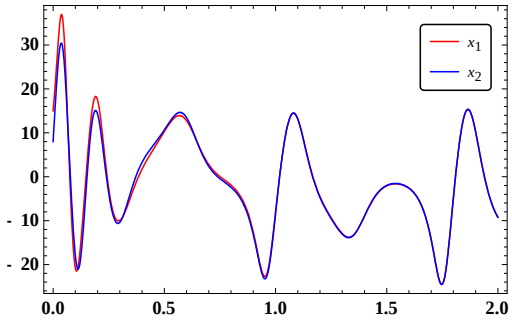

Figure 11: Time Series of x_1 & x_2 for nonidentical synchronizatior

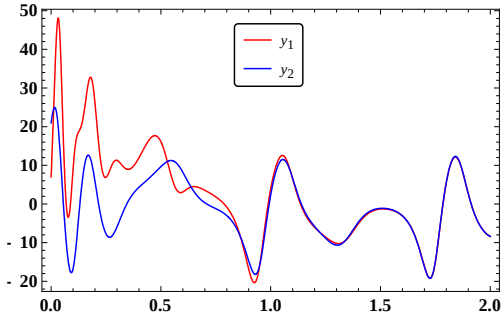

Figure 12: Time Series of y_1 & y_2 for nonidentical synchronizatior

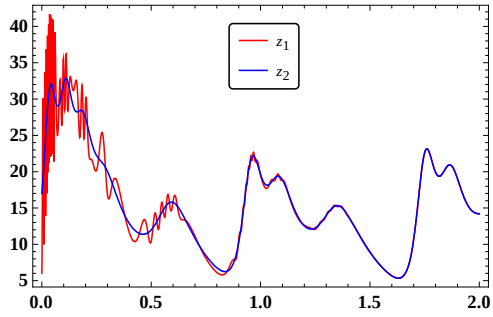

Figure 13: Time Series of z_1 & z_2 for nonidentical synchronizatior

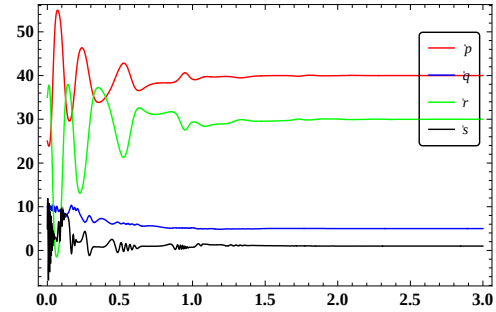

Fig 14: Time Series of $\dot{p}, \dot{q}, \dot{r}$ & $\dot{s}$ for nonidentical Synchronizatior

Figure 5 presents the time derivative of the LEF for the controlling of chaos in system [18] that characterizes that the new system is dissipative $\left(\dot{V}(e) < 0\right)$. The time series of the state vectors of the two identical chaotic systems (16) and (17) to observe the synchronization. Figure 9 depicts the time history of the parameters estimates for synchronization of the two identical chaotic systems [18] under the update law (26). The evolution of the synchronized errors with response system parameters unknown is depicted in Fig. 10. Figures 11-13 elaborate the time history of state vectors of the two nonidentical chaotic systems ([18], [24]).

Fig. 15 illustrates the times history of the parameters estimates p, q, r, and s and α, β, γ and δ respectively of the two nonidentical chaotic systems ([18], [24]) under the update law (36) with initial estimated parameters $\alpha_1(0) = 5$, $\beta_1(0) = 10$, $\gamma_1(0) = 2$ and $\delta_1(0) = 1$.

For the two different chaotic systems ([18]) and [24]), that contain parameters mismatches and different structures, the feedback controllers were utilized to synchronize the states of master and slave systems asymptotically when the controls are switched on at t = 0 s. It has been shown that the Liu chaotic system is forced to track the new chaotic system

and the states of two different chaotic systems show similar behavior, which shows that the error system (Fig. 16) is feedback stabilized and the investigated controllers are more robust to accidental mismatches in the transmitter and receiver. Moreover, Fig. 17 demonstrates derivative of the LEFs of identical chaotic systems [18] and nonidentical chaotic systems ([18] and [24]). The synchronization with negative derivative of the LEFs confirms that the divergence of the flows (23) and (34) are dissipative $\left(\dot{V}(e)<0\right)$ that allows large synchronizable interval, which is especially significant for secure communication and engineering applications etc.

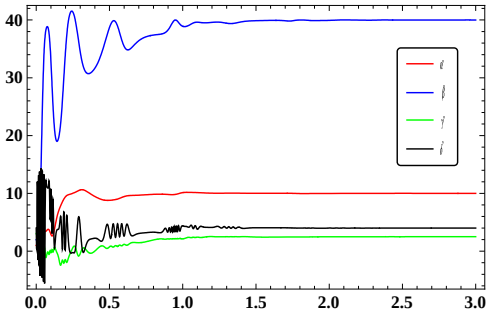

Fig 15: Time Series of $\dot{e}$, $\dot{f}$, $\dot{g}$ & $\dot{h}$ for nonidentical Synchronizatio

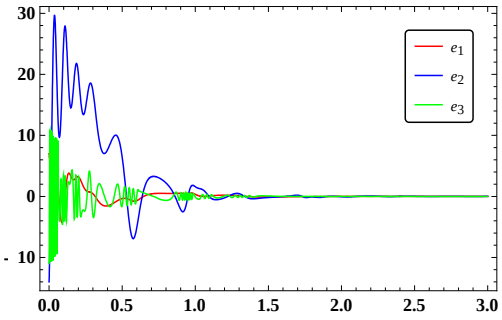

Figure 16: Time Series of errors for nonidentical Synchronizatio

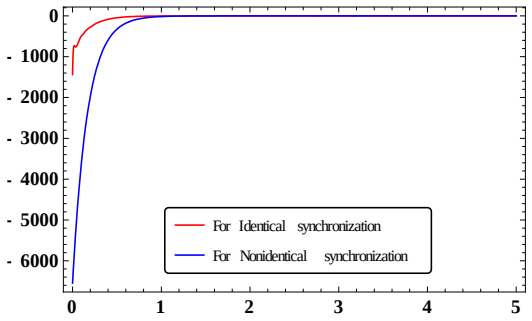

Figure 17: Time Series of Lyapunov errors functions

V. Summary and Conclusion

In this research, the Adaptive Controllers have been designed to repress the chaos to its equilibrium point at the origin. The synchronization between two identical and two nonidentical 3-D chaotic systems with fully unknown parameters has also been achieved. Based on the Lyapunov Direct Method, the Adaptive control laws for synchronization controllers associated with the Adaptive update laws of system parameters were devised to make the states of two identical and two completely different chaotic systems asymptotically synchronized. The accuracy and efficiency of the proposed controllers have been demonstrated and are validated by the numerical simulations. Furthermore, the synchronization with negative derivative of the PDQLE functions allows substantial synchronizable interval, which is especially important for engineering applications.

One can observe that the convergence of the systems parameters and the synchronization errors are obtained with good accuracy. The chaos control and synchronization of two identical as well as nonidentical chaotic systems presumes potential applications in the field of nonlinear sciences. The obtained results of our current study could to be found in good agreement with experimental observations and can be employed by those researchers involved in the field of secure communication, chaotic modulation and chaotic masking etc.

However, there is always some external disturbances or internal noise exits in real plants that might cause instability and poor performance. Similarly, it is also difficult to determine exactly the values of the system parameters and the controller gain *k* cannot be properly chosen to guarantee the stability of the controlled system. Hence, future work needs to address these issues to extend the capability of the system and its circuitry design for various applications in different fields such as engineering, hybrid image encryption, secure communications and genetic networks.

VI. Acknowledgment

The authors are very grateful to the referee(s) for their valuable comments and suggestions which led to an improvement of this research paper.

References

[1] S. Boccaletti, C. Grebogi, Y. C. Lai, H. Mancini, D. Moza, "The control of chaos: theory and applications", *Physics reports*, vol. 329: pp. 103-197, 2000.

[2] I. Pehlivan, Y. Uyaroglua, "A new chaotic attractor from General Lorenz system family and its electronic experimental implementation", *Turk Jour. of Elec. Eng. & Comp. Sci*, vol. 18, no. 2, 2010.

[3] E. Ott, C. Grebogi, J. A. Yorke, *Controlling Chaos*, *Phys. Rev. Lett.*, vol. 64, pp. 1196-1199, 1990.

[4] K. Pyragas, V. Pyragas, I. Z. Kiss, J. L. Hudson, "Adaptive control of unknown unstable steady states of dynamical systems", *Phy. Rev. E* vol. 70, 2004.

[5] L. M. Pecora, T. L. Carroll, "Synchronization in Chaotic Systems", *Phys. Rev. Lett*., vol 64, no. 8, pp. 821–825, 1990.

[6] A. Saaban, A. Ibrahim, M. Shahzad, I. Ahmad, "Identical Synchronization of a New Chaotic System via Nonlinear Control and Linear Active Control Techniques: A Comparative Analysis", *International Journal of Hybrid Information Technology*, vol. 7, no. 1, pp. 211-224, 2014.

[7] L. O. Chua, M. Komuro, S. Tanaka, "Simplest chaotic nonautonomous circuit", *Phys. Rev. A*, vol. 30, pp. 1155-1158, 1984.

[8] I. Ahmad, A. Saaban, A. Ibrahim, M. Shahzad, "Global Chaos Synchronization of Two different Chaotic Systems Using Nonlinear Control", *International Journal of Sciences: Basic and Applied Research* (*IJSBAR*), vol. 13, no. 1, pp. 225-238, 2014.

[9] B. Idowu, U. Vincent, A. Njah, "Generalized Adaptive Backstepping Synchronization for Non-identical Parametrically Excited Systems", *Nonlinear Analysis: Modelling and Control*, vol. 18, no. 1, pp. 112–128, 2013.

[10] K. S Ojo, A. Njah, S. Ogunjo, "Comparison of backsteeping and modified active control in projective synchronization of chaos in an extended Bonhoffer-van der Pol Oscillator", *Pranama Journal of Physics*, vol. 80, no. 5, pp 825-835, 2013.

[11] J. Xing, "Adaptive hybrid function projective synchronization of chaotic systems with fully unknown periodical time-varying parameters", *Nonlinear Analysis: Modelling and Control*, vol. 18, no. 1, pp 112–128, 2013.

[12] S. Vaidyanathen, "Adaptive Control and Synchronization of Shimizu-Morioka Chaotic System", *International Journal in Foundations of Computer Science & Technology*, vol. 2, no. 4, pp 29-42, 2012.

[13] O. Olusola, "Adaptive Synchronization of identical and Nonidentical Hyperchaotic Systems with unknown Parameters", *The African Review of Physics*, vol. 7, pp 345-352, 2012.

[14] M. Ali Khan, "Adaptive Synchronization of two coupled Netwon-Leipnik System with Uncertain Parameter", *Int. Journal of Basic and Applied Sciences*, vol. 1., no. 4, pp 439-447, 2012.

[15] S. Vaidyanathen, K. K. Rajagopal, "Global Chaos Synchronization of Hyperchaotic Pang and Hyperchaotic Wang Systems via Adaptive Control", *Int. Journal of Soft Computing*, vol. 7, no. 1, pp 28-37, 2012.

[16] H. Zhang, X. Ma, B. Xue, "A novel boundedness-based linear and nonlinear approach to control chaos", *Chaos, Solitons and Fractals*, vol. 22, pp 433-442, 2004.

[17] S. Al-Hadhrami, A. Saaban, A. Ibrahim, M. Shazad, I. Ahmad, "Linear Active Control Algorithm to Synchronize a Nonlinear HIV/AIDS Dynamical System", *Asian Journal of Applied Sciences and Engineering*, vol. 3, no. 2, pp 96-115, 2014.

[18] C. Li, L. Wu, H. Li, Y. Tong, "A novel chaotic system and its topological horseshoe", *Nonlinear Analysis, Modelling and Control*, vol. 18, no. 1, pp 66–77, 2013.

[19] H. K. Khalil, *Non Linear dynamical Systems*, Prentice Hall, 3rd Ed, NJ 07458, USA, 2002.

[20] M. Aghababa, H. Aghababa, "Synchronization of nonlinear chaotic electromechanical gyrostat systems with uncertainties", *Nonlinear Dyn*, vol. 67, pp 2689-2701, 2012.

[21] Z. Xinghua, D. Shougang, "Adaptive Chaos Synchronization for a Type of Non-Smooth-Air-Gap Permanent Magnet Synchronous Motors", *Control and Decision Conference*, 2008, Ding Shougang, China.

[22] M. Ying-Ying, L. Yun-Gang, "Barbalat's Lemma and its application in analysis of system stability", *Journal of Shandong University of Technology*, vol. 37, no. 1, pp 51-55, 2007.

[23] L. Nguyen, K. Hong, "Adaptive Synchronization of two coupled chaotic Hindmarsh-Rose Neurons by controlling the membrane potential of a slave neuron", *Applied Mathematical Modeling*, vol. 37, no. 4, pp 2460-2468, 2013.

[24] T. Zhou, G. Chen, "Classification of Chaos in 3-D Autonomous Quadratic System-1. Basic Framework and Method", *International Journal of Bifurcation and Chaos*, vol. 16, no. 9, pp 2456-2479, 2006.

Mitigating the Effects of Mobility and Synchronization Error in OFDM Based Cooperative Communication Systems

Yetera B. Bereket, Philip K. Langat, and Edward K. Ndungu

***Abstract*— An Orthogonal Frequency Division Multiplexing based mobile wireless network with a sender, a destination and a third station acting as a cooperating node is modelled and analyzed. The length of cyclic prefix in the orthogonal frequency division multiplexed symbols is made to vary depending on the channel conditions and maximum likelihood estimator is used at the receiver in order to compensate for the carrier frequency offset that occurs during transmission. Simulation results show that maximum likelihood estimator has better performance than self-cancellation estimations. The channels between the source, the cooperating node and the destination are modelled containing thermal noise, Rayleigh fading, Rician fading and path loss. Amplify-and-Forward cooperation protocol is used at the cooperating node when the system is in cooperation mode. For a relatively short distance between the cooperating nodes, when compared to the distance between them and the base station, amplify and forward cooperation protocol has a better performance than decode-and forward protocol, unless an error correcting code is simulated. The cooperating node turns its cooperation mode switch ON or OFF depending on the channel state between the source and the cooperating nodes. The performance of different combination protocols at the receiver is simulated and maximum ratio combining is found to have better performance. However, for immobile wireless sensor networks Extended SNR (ESNR) combiner has also better performance. The system has also showed that with any kind of combination protocol at the receiver it is possible to achieve second order diversity when there is only one cooperating node in the system.**

***Keywords*— OFDM, CFO, ICI, cyclic prefix, cooperative communication, BER, SNR, maximum ratio combiner, amplify-and forward, decode-and-forward, subcarriers, maximum likelihood.**

I. Introduction

During the last two decades, the wireless communications have experienced a huge growth in both capacity and variety. This growth has been possible to achieve due to some advancement and new discoveries of communication technologies, techniques and protocols. The mere motivation that stimulated intense interest to the advancement of existing technologies in wireless communication systems is an increased demand for services that need higher data rate and higher capacity. It has been seen and still expected that the wireless communication systems of the near future will require data rates up to few hundreds of mega bits per second (Mbps), which are able to deliver bandwidth hungry applications such as online gaming, virtual class room, and video streaming. The required data rate of the next generation wireless communication systems will be achieved by efficiently increasing the amount of the allocated bandwidth and using more advanced technologies, both in hardware and software.

One of the major themes in today's broadband systems is the use of orthogonal frequency division multiplexing (OFDM). Orthogonal frequency division multiplexing is a modulation scheme suitable for frequency selective channels and for providing high speed data transmission, which makes it one of the promising solutions for the next generation wireless communications. OFDM mitigates the effect of multipath channel by essentially dividing the source spectrum into many narrow sub-bands that are transmitted simultaneously. In OFDM system, the source bit-stream to be transmitted over the air link is split into N parallel streams, which are later going to be modulated using N sub-carriers. Because of using many sub-carriers, the symbol duration T_s becomes N times larger. This reduces and even totally averts the effect of inter symbol interference (ISI) in multipath channels, and thereby reduces the equalization complexity. However, there is a need for more developments of OFDM systems in terms of complexity reduction and adaptation, therefore reconfigurable solutions are needed to achieve the user requirements. This is necessary because the end users require lightweight, compact size and power efficient devices besides the high bit rate capabilities.

Furthermore, combining OFDM transmission technique with the new techniques such as multiple-input-multiple-output (MIMO) or cooperative communication can also enhance the capacity and the bit rate of the emerging wireless communication systems. Also MIMO transmissions have been extensively studied as a means to improve spectral efficiency in wireless networks. While MIMO techniques offer tremendous advantages, its performance strongly depends on the number of antenna elements, spatial fading correlations between antennas, the presence of line of sight component, etc. Especially, multiple antennas at small handsets/cellular phones are unattractive for the achievement

Manuscript received September 10, 2014, revised October 26, 2014.

Yetera Bereket, Department of Electrical Engineering, Pan African University of Science Technology and Innovation(Correspondence: berryboyy@yahoo.com)

K. Langat, Department of Telecommunication and Information Systems, Jomo Kenyatta University of Agriculture and Technology

Edward K. Ndungu, Department of Telecommunication and Information Systems, Jomo Kenyatta University of Agriculture and Technology

doi: 10.11601/ijates.v3i2.97

of transmit/receive diversity due to the limitation on size, power, hardware and price. The advantages of MIMO techniques can be achieved via cooperative communication. However, carrier frequency offset plays an important role when OFDM is integrated into cooperative communication systems [1]. Carrier frequency offset (CFO) arises either due to mobility that results in different Doppler shifts for each relay, or due to oscillator instabilities that result in slightly different carrier frequencies for every relay. This CFO leads to inter carrier interference, which is the leakage of signal power, in any OFDM based communication system.

In the context of addressing CFO issues surrounding cooperative communication systems based on OFDM, much of the work to date has focused on cooperative relaying techniques that utilize orthogonal space-time codes. For instance, in [1], [2] the authors design appropriate receivers to handle frequency offsets. In [1], the authors develop a frequency synchronization algorithm that exploits the structure of the cooperation protocol. In [2], the authors utilize a long cyclic prefix to mitigate the impact of carrier frequency offsets. This technique reduces the transmission bit rate. One mechanism of simplifying the receiver and transmitter design is to assign orthogonal subcarriers to each relay. The design of frequency offset estimation algorithms were considered in [3] from a multiuser perspective whereby each user is assigned a unique set of subcarriers. The other widely known carrier frequency offset mitigation technique is the self-cancellation (SC) technique [4]. The main idea in self-cancellation is to modulate one data symbol onto a group of subcarriers with predefined weighting coefficients to minimize the average carrier to interference ratio (CIR). This is the main drawback of this method because it utilizes half of the available subcarriers for CFO estimation and hence, inter carrier interference reduction.

Cooperative communication networks [5, 6 and references therein] are created via the help of cooperating terminals which are willing to help the communication of any source-destination pair. End to end spectral efficiency of a wireless network can be increased with the aid of cooperative strategies. The concept of node cooperation brings a new form of diversity. Transmit and/or receive diversity can be achieved even with single antenna terminals [7]. By this way, the need for costly multiple transceiver circuitry diminishes. Furthermore, spatial fading correlation of a cooperative diversity scheme is expected to be much less than spatial fading correlation of multi-antenna arrays co–located at a terminal.

In a cooperative communication system, each wireless user is assumed to transmit data as well as act as a cooperative agent for another user. One of the key components in such a cooperative relay network is a forwarding method used by a relay terminal. Amplify-and-Forward (AAF) and Decode-and-Forward (DAF) are the main forwarding protocols which can be used in the cooperative relay networks [7]. A relay terminal using the AAF scheme amplifies and forwards the signal received from its immediate predecessor (the source node) in the network. A relay terminal using the DAF protocol decodes, re-encodes and forwards the signal received from its immediate predecessor in the network. The use of either AAF or DAF at a relay terminal achieves different performance results under given Signal to Noise Ratio (SNR) conditions. But when the cooperating node gets the line-of-sight signal from the source node, AAF cooperation protocol is preferable than the DAF protocol because of its simplicity and it also doesn't incur system losses in terms of introducing processing delay.

With an intent to integrate the benefits of both cooperation as well as OFDM, OFDM based cooperative communication networks have been intensely investigated [8]-[13]. In [8], [9] Gui and Cimini Jr devise bit loading algorithms for cooperative OFDM systems with decode-and-forward (DF) cooperation protocol, considering a single source-destination pair and multiple cooperating nodes. In [10], the authors proposed an OFDM-based selective relaying scheme in a multihop cooperative network, where the relay selection at each hop is performed on a per-subcarrier basis and joint selection is adopted at the last two hops. In [11], Jamshidi *et al*. derive exact expression and tight lower bound for the outage probability of space-frequency coded cooperative OFDM system. Effect of carrier frequency offsets on the relay-to-destination links in cooperative OFD is investigated in [12]. In [13], interference mitigation techniques to alleviate the effect of inter-symbol interference (ISI) and inter-carrier interference (ICI) caused due to frequency selectivity of the channel and violation of 'quasi-static' assumption in space-frequency block coded cooperative OFDM are presented and analyzed for amplify-and-forward (AAF) and decode-and-forward (DAF) cooperation protocols.

In this paper an OFDM based cooperative communication system with AAF protocol is developed. In order to completely avert the effect of ISI from occurring some redundant information are added into the OFDM symbols before transmission. This added redundant information is called cyclic prefix (CP). Maximum likelihood (ML) estimation is used to estimate the CFO and compensate for its effect that occurs due to the Doppler shift and transmitter-receiver carrier frequency offset. ML estimation is compared with the self-cancellation (SC) estimation series and is found to be better in many aspects. The cooperating node is assumed to get line-of-sight signal from the source and hence, the channel between the cooperating nodes is assumed to have Rician fading characteristics. The channels between the source node and the receiver and the cooperating node and the receiver as well are assumed to be frequency selective and Rayleigh fading. We also assumed the cooperating node to be only a few meters apart (up to 10 meters) from the source node. This is due to the fact that the cooperating nodes need to be a few wavelengths apart in order to create a virtual MIMO system through spatial diversity. In most cases, if the distance between the source and cooperating nodes is longer than 10 meter the level of the noise added to the transmitted signal will become pronounced and eventually surpass the threshold value. In addition to this, by limiting the distance between the two cooperating nodes to 10 meter, the channel characteristics of source node to destination and cooperating node to destination will be nearly the same. Hence, the carrier frequency offset estimated at the receiver upon the arrival of

a signal from the source node will be used to compensate for the effects of CFO on both channels, the channel between the source node and the destination and the channel between the cooperating node and the destination. Meaning, there is no need to estimate the CFO that occurs over the cooperating node to destination channel. This minimizes computational time and complexity at the receiver side.

Our contributions are three-fold. First, we show through simulation results that cooperative communication systems with amplify and forward cooperation protocols are not affected by the carrier frequency offset of the relaying nodes when the distance between the cooperating nodes is limited to be in the range of 10 meter. That is, the final received signal at the destination is only affected by the carrier offset between the source and destination, much like relay-less system. This is significant finding which shows that from the point of view of the destination, it can use a receiver built for a conventional multiple antenna transmissions without employing a multiuser-like front-end to handle non coherent transmissions from multiple nodes.

The second contribution is that when the distance between the cooperating nodes is limited to 10 meter range, there will be no need to deal with the issues of imperfect timing synchronization. Hence, in these types of cooperative communication systems, perfect timing synchronization can be assumed between the cooperating nodes. And, since the cooperating node is located far enough from the source node, there will be no spatial fading correlation between the channels from the source to the destination and from cooperating node to the destination. These reduce computational complexity at the cooperating node and at the intended destination.

Lastly, we analyzed, and build a fully functional amplify-and-forward cooperative communication system which is based on an OFDM transmission technique. We have come up with new threshold value at the cooperating node based on which the cooperating node decides whether to cooperate with the source node. In most OFDM cooperative networks to date, the cooperating node amplifies and retransmits the received signal together with the noise added to the signal. In such cases the original message signal will be overshadowed by the noise signal when it reaches the intended destination and it will have no meaning. Through the simulation results, we have also shown how the performance of such systems improves when the cooperating node gets the line-of-sight signal from the source node.

Generally, the solutions developed in this paper to mitigate the effects of CFO in a cooperative OFDM system have shown an advantage of improving system performance in terms of bit error rate (BER) against signal-to-noise ratio (SNR). To validate the achieved results, section VI compares the performances of the system developed in this paper with the widely known and used cooperative OFDM system with self-cancellation CFO estimator.

II. SIGNAL MODEL

The signal to be transmitted over the wireless channel must first be converted into OFDM symbols. In OFDM system with N subcarriers, N information symbols are used to construct one OFDM symbol. Each of the N symbols is used to modulate a subcarrier and the N modulated subcarriers are added together to form an OFDM symbol. Orthogonality among subcarriers is achieved by carefully selecting the carrier frequencies such that each OFDM symbol interval contains integer number of periods for all subcarriers. Using discrete-time baseband signal model, one of the most commonly used schemes is the IDFT-DFT based OFDM systems [14]. Guard time, which is cyclically extended to maintain inter-carrier orthogonality, is inserted that is assumed longer than the maximum delay spread to totally eliminate inter-symbol-interference [15]. In the presence of virtual carriers, only M out of N carriers is used to modulate information symbols. Without loss of generality, we assume that the first M carriers are used to modulate information symbol, while the last $N - M$ carriers are virtual carriers. With symbol rate sampling, the discrete time OFDM model is:

$$s(n) = \frac{1}{\sqrt{N}} \sum_{k=0}^{N-1} d_k \mathrm{e}^{j2\pi nk/N} , \quad (1)$$

where each d_k is used to modulate the subcarrier $\mathrm{e}^{j2\pi nk/N}$. Written in matrix form, we have:

$$s = \mathbf{W}\mathbf{d} , \quad (2)$$

where $\mathbf{W}$ consists of the first M columns of the IDFT matrix and $d = [d_0,\ldots, d_{M-1}]$ is the symbol vector. In the presence of time dispersive channel, additive noise, and carrier frequency offset, the OFDM signal at the receiver is now:

$$x(n) = \frac{1}{\sqrt{N}} \sum_{k=0}^{N-1} d_k H(k) \mathrm{e}^{j(2\pi k/N + \Delta\omega T_s)n} + z(n) , \quad (3)$$

where $H(k)$ is the channel frequency response corresponding to subcarrier k, $z(n)$ is additive complex Gaussian noise, and $T_s = T/N$ is the symbol interval with T being the IDFT interval (or OFDM symbol interval, excluding the guard time, as often termed in the literature). Here the initial phase due to frequency offset is assumed to be zero (equivalently, the initial phase can be absorbed into $H(k)$). Notice if we define $\varphi = \Delta\omega \cdot T_s$, then φ and the frequency offset $\Delta\omega$ differ only by a constant scalar, hence estimation of $\Delta\omega$ is equivalent to estimation of the normalized phase shift φ.

III. III. OVERALL SYSTEM MODEL

Consider a three node OFDM based cooperative communication network with source node (SN), cooperating node (CN) and receiving node (RN). The SN broadcasts its signal over the fading wireless communication channel and both the CN and RN receive the signal. The CN amplifies and re-transmits the received signal depending up on the link state between its node and the SN and also if the cooperating switch is on ON state by the time the signal arrives. It is assumed that the source and cooperating nodes are always near to each other and the cooperating node gets the LOS signal from the source node. Hence, the channel between the source node and the cooperating node assumed to have Rician fading characteristics. The channels between the source node and the receiving node and between the cooperating node and the receiving node are assumed to be

frequency selective and Rayleigh fading.

Consider N OFDM subcarriers. In the first time slot, SN transmits one OFDM frame of duration $(N + N_g)T_s$, where T_s is one sample duration and N_g is the cyclic prefix (CP) length. The transmitted OFDM frame consisting of data symbols $X[k]$, $k = 0,1,\ldots,N-1$, is given by:

$$x[n] = \frac{1}{N}\sum_{k=-N_g}^{N-1} X[k]\mathrm{e}^{j2\pi kn/N}\ ;\ -N_\mathrm{g} \le n \le N-1. \tag{4}$$

Let $h_{sc}[n]$, $h_{sr}[n]$ and $h_{cr}[n]$ denote the channel impulse responses (CIR) of the source node to cooperating node, the source node to the receiving node and the cooperating node to the receiving node links, respectively. The received OFDM symbols at the cooperating and receiving nodes, during the first phase (time slot), will be:

$$y_{sc}[n] = x[n] * h_{sc}[n] + n_{sc}[n], \tag{5}$$

$$y_{sr}[n] = x[n] * h_{sr}[n] + n_{sr}[n], \tag{6}$$

where $*$ indicates linear convolution, $n_{sc}[n]$ is the white Gaussian noise signal at the cooperating node, and $n_{sr}[n]$ is the white Gaussian noise signal at the receiving node, both white Gaussian noises with variance N_o; $y_{sc}[n]$ is the signal received at the cooperating node from the source node and $y_{sr}[n]$ is the signal received at the destination from the source node. During the second time slot (or cooperation phase), the cooperating node will amplify the received signal by gain β and re-transmits it to the receiving node. Hence, the received signal at the receiving node, $y_{cr}[n]$, in this second phase is:

$$\begin{aligned} y_{cr}[n] &= \beta y_{sc}[n] * h_{cr}[n] + n_{cr} = \\ &= \beta\big(x[n] * h_{sc}[n] + n_{sc}[n]\big) * h_{cr}[n] + n_{cr}, \end{aligned} \tag{7}$$

where $*$ indicates linear convolution and n_{cr} is the white Gaussian noise over the cooperating and receiving nodes link with variance N_o. The magnitude of the amplifying factor is determined based on the transmitted signal energy and the received signal energy. Let $\xi = E[|x[n]|^2]$, then the energy of the signal received at the cooperating node is:

$$\begin{aligned} E[|y_{sc}[n]|^2] &= E[|h_{sc}[n]|^2]E[|x[n]|^2] + E[|n_{sc}[n]|^2] = \\ &= E[|h_{sc}[n]|^2]\xi + 2N_o. \end{aligned} \tag{8}$$

To re-transmit the data with the same power as the source node did, the cooperating node needs to amplify the received signal by a factor of:

$$\beta = \sqrt{\frac{\xi}{E[|h_{sc}[n]|^2]\xi + 2N_o}}. \tag{9}$$

The system developed in this paper supports cooperation if and only if $\xi >> E[|h_{sc}[n]|^2]\xi + 2N_o$, otherwise the cooperating node turns its cooperation mode switch to OFF state. Therefore, the received signal at the receiving node in two time slots is:

$$\begin{aligned} y[n] &= y_{sr}[n] + y_{cr}[n] = \\ &= \big(x[n] * h_{sr}[n] + n_{sr}[n]\big) + \\ &\quad + \beta\big(x[n] * h_{sc}[n] + n_{sc}[n]\big) * h_{cr}[n] + n_{cr} = \\ &= x[n] * h_{sr}[n] + \beta x[n] * h_{sc}[n] * h_{cr}[n] + \\ &\quad + \beta n_{sc}[n] * h_{cr}[n] + n_{sr}[n] + n_{cr}[n]. \end{aligned} \tag{10}$$

Using distributive property of convolution and defining $w[n]$ as $w[n] = \beta n_{sc}[n] * h_{cr}[n] + n_{sr}[n] + n_{cr}[n]$, the eqn. (10) can be written as:

$$y[n] = x[n] * \big(h_{sr}[n] + \beta h_{sc}[n] * h_{cr}[n]\big) + w[n]. \tag{11}$$

The output on the k^{th} subcarrier is given by performing the discrete Fourier transform on the above equation (11).

Defining $h_r[n] = h_{sr}[n] + \beta h_{sc}[n] * h_{cr}[n]$, then (11) becomes $y[n] = x[n] * h_r[n] + w[n]$. Then:

$$Y[k] = X[k]H_r[k] + W[k], \tag{12}$$

where $H_r[k] = H_{sr}[k] + \beta H_{sc}[k]H_{cr}[k]$, whereas $H_{sr}[k]$ and $H_{sc}[k]$ being the N-point DFTs of $h_{sr}[n]$ and $h_{sc}[n]$, respectively. Equation (12) shows the amplitude of the transmitted signal is attenuated by a factor of $H_r[k]$ and interfered by a signal $W[k]$. To reduce this reduction in amplitude and mitigate the interference at the destination this paper used different type of combiners and analysed the performance of each combiner.

The schematic diagram in Fig. 1 shows the overall system followed by its description. The transmitting node should always perform signal modulation whenever it has a signal to transmit. Hence the bit stream will be converted into symbols. Then the source node performs serial to parallel conversion. The number of parallel symbols should coincide with the number of available subcarriers. After the conversion, IFFT is performed to obtain OFDM symbol. The cyclic prefix (CP) is lastly added before transmission to completely avert inter-symbol interference (ISI) and minimize Inter Carrier Interference (ICI) at the receiving end. Then the transmitter in the source node converts the parallel data into serial data and transmits it over the air link to the cooperating node and the receiving node. In this first phase, the cooperating node performs amplification of the received signal for re-transmission if the received signal passes the threshold quality for re-transmission. The cooperating node decides to cooperate depending on the state of the channel between the source and cooperating nodes. In the second phase, the receiver receives another copy of the signal from the cooperating node and combines it with the signal received from the source node directly using maximum ratio combiner (MRC). In this paper we have checked and tested different combiners under different conditions. After obtaining the received signal by combining the direct signal and the signal from the cooperating node by maximum ratio combiner, the process that was undertaken in the main transmitting node is reversed to obtain the decoded data. The CP is removed to obtain the data in the discrete

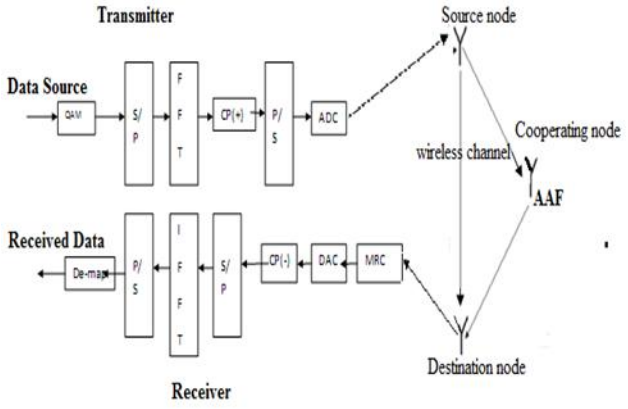

Figure 1: OFDM based Cooperative communication system diagram.

time domain and then processed using the FFT for data recovery. Since the wireless channel is known to be fading and to introduce Doppler shift, the ML estimator that comes immediately after the FFT block in the system is used to perform CFO estimation. Then using the estimated values of CFO, the ICI that occurs during transmission will be compensated. Finally the symbols pass through the de-mapper (demodulation) in order to regenerate the received bit stream.

IV. Maximum Likelihood Estimation for CFO at the Receiver

In this paper the source node and the cooperating node are assumed to be separated only few meters apart (up to 10 meters maximum) and the cooperating node gets the LOS signal from the source node. Hence, it is also assumed that the channel characteristics between the cooperating node and the receiver are the same with the channel characteristics of the source node to the receiver, except for simulation less Doppler frequency for the cooperating node-to-receiver channel is used. This is due to the fact that only a node with lower speed will be chosen for cooperation. Therefore, the CFO estimated at the receiver for the signal coming from the source node will be used to compensate both the signal from the source and cooperating nodes. That means, there is no need to do CFO estimation for the signal arriving at the receiver from the cooperating node.

This method has been presented in several papers in slightly varying forms [16, 17]. The training information required is at least two consecutive repeated symbols. The IEEE 802.11a preamble satisfies this requirement for both the short and long training sequence. Let the transmitted baseband signal be s_n, then the complex baseband model of the passband signal y_n is:

$$y_n = s_n \mathrm{e}^{j2\pi f_{tx} n T_s}, \tag{13}$$

where f_{tx} is the transmitter carrier frequency and T_s is the sampling interval. After the receiver down-converts the signal with a carrier frequency f_{rx}, the received complex baseband signal r_n is:

$$r_n = s_n \mathrm{e}^{j2\pi f_{tx} n T_s} \mathrm{e}^{-j2\pi f_{rx} n T_s} + w_n = s_n \mathrm{e}^{j2\pi \Delta f n T_s} + w_n, \tag{14}$$

where $\Delta f = f_{tx} - f_{rx}$ is the carrier frequency offset and w_n the white Gaussian noise with variance N_o.

Let D denote the delay between the identical samples of the two repeated symbols. Then the frequency offset estimator is developed as follows: The cross-correlation of the two consecutive symbols is computed as:

$$\begin{aligned} c &= E\left[\sum_{n=0}^{N-1} r_n r_{n+D}^*\right] = \\ &= E\left[\sum_{n=0}^{N-1}\left(s_n \mathrm{e}^{j2\pi\Delta f n T_s} + w_n\right)\left(\left(s_{n+D}\mathrm{e}^{j2\pi\Delta f (n+D)T_s} + w_{n+D}\right)^*\right)\right]. \end{aligned} \tag{15}$$

Since w_n is an additive white Gaussian noise white mean zero and covariance σ^2, the above equation will reduce to:

$$\begin{aligned} c &= \sum_{n=0}^{N-1} s_n s_{n+D}^* \mathrm{e}^{j2\pi\Delta f n T_s} \mathrm{e}^{-j2\pi\Delta f (n+D)T_s} = \\ &= \mathrm{e}^{-j2\pi\Delta f D T_s} \sum_{n=0}^{N-1} s_n s_{n+D}^* = \mathrm{e}^{-j2\pi\Delta f D T_s} \sum_{n=0}^{N-1} |s_n|^2. \end{aligned} \tag{16}$$

Hence, the maximum likelihood estimate gives us the frequency offset estimation as:

$$\Delta f = \frac{\arg(c)}{2\pi D T_s}. \tag{17}$$

The ML estimation of frequency offset can also be derived after the discrete Fourier Transform (DFT) processing (i.e. in frequency domain). The received signal during two repeated symbols is (ignoring noise for convenience):

$$r(n) = \frac{1}{N}\left[\sum_{k=-K}^{K} X_k H_k \mathrm{e}^{j2\pi n(k+f_r)/N}\right], \text{ for } n = 0,...2N-1 \tag{18}$$

where X_k's are the transmitted data symbols, H_k is the channel frequency response for the k^{th} subcarrier, K is the total number of subcarriers, and f_r is the relative frequency offset to the subcarrier spacing. The DFT of the first symbol and for the k^{th} subcarrier is:

$$R_{1,k} = \sum_{n=0}^{N-1} r_n \mathrm{e}^{-j2\pi kn/N}, \; k = 0,1,...N-1. \tag{19}$$

The DFT of the second symbol is derived as:

$$R_{2,k} = \sum_{n=N}^{2N-1} r_n \mathrm{e}^{-j2\pi kn/N} = \sum_{n=0}^{N-1} r_{n+N} \mathrm{e}^{-j2\pi kn/N}, \; k = 0,...N-1. \tag{20}$$

But from (14) the received signal at the index of $n + N$, $r(n + N)$, is given as:

$$\begin{aligned} r(n+N) &= \frac{1}{N}\sum_{k=-K}^{K} X_k H_k \mathrm{e}^{j2\pi(n+N)(k+f_r)/N} = \\ &= \frac{1}{N}\sum_{k=-K}^{K} X_k H_k \mathrm{e}^{j2\pi n(k+f_r)/N} \mathrm{e}^{j2\pi(k+f_r)}. \end{aligned} \tag{21}$$

Since $\mathrm{e}^{j2\pi(k+f_r)} = \mathrm{e}^{j2\pi k}\mathrm{e}^{j2\pi f_r}$ and $\mathrm{e}^{j2\pi k} = 1$ for all integer values of k, eqn. (21) can be rewritten as:

$$\begin{aligned} r(n+N) &= \frac{1}{N}\sum_{k=-K}^{K} X_k H_k \mathrm{e}^{j2\pi n(k+f_r)/N} \mathrm{e}^{j2\pi f_r} = \\ &= r(n)\mathrm{e}^{j2\pi f_r}, \; n = 0,1,...2N-1. \end{aligned} \tag{22}$$

Substituting equation (22) into equation (20) yields:

$$R_{2,k} = \sum_{n=0}^{N-1} r(n) e^{j2\pi f_r} e^{-j2\pi kn/N} = \\ = e^{j2\pi f_r} \sum_{n=0}^{N-1} r(n) e^{-j2\pi kn/N} = \\ = R_{1,k} e^{j2\pi f_r}, \quad k = 0, 1, ...N-1. \tag{23}$$

This, therefore, shows us that every subcarrier experiences the same shift that is proportional to the frequency offset. The cross-correlation of the two subcarriers is obtained as follow:

$$C = \sum_{k=-K}^{K} R_{1,k} R_{2,k}^{*} = \sum_{k=-K}^{K} R_{1,k} \left(R_{1,k} e^{j2\pi f_r} \right)^{*} = \\ = e^{-j2\pi f_r} \sum_{k=-K}^{K} R_{1,k} \left(R_{1,k} \right)^{*} = e^{-j2\pi f_r} \sum_{k=-K}^{K} \left| R_{1,k} \right|^2. \tag{24}$$

Thus, the frequency offset estimator governing equation is:

$$f_r = -\frac{1}{2\pi} \arg(C), \tag{25}$$

$$\Delta f = -\frac{f_{sc}}{2\pi} \arg(C), \tag{26}$$

which is quite similar in form to the time domain version of the ML estimation in (17).

This CFO estimation is used at the receiver to estimate the carrier frequency offset, that occurs due to Doppler shift and frequency synchronization error of the transmitter and receiver. Then this estimated CFO values will be used to compensate both the signals from the source node and the cooperating node at the receiver node.

V. Simulation Results and Discussion

For simulation, quadrature amplitude modulation (QAM) scheme with $M = 4$ is chosen and the total number of subcarriers is set to 64. These parameters are chosen because the current wireless communication systems, 3G and beyond, are based on them. The fading channel between the source node and the receiver and the fading channel between the cooperating node and the receiver are set to have six different signal propagation paths with 100 Hz and 80 Hz Doppler frequency, respectively. The 100 Hz Doppler shift between the source node and the base station is the worst case in wireless communication system. The reason we chose 80 Hz Doppler frequency between the cooperating node and the base station is that the source node is always assumed to select a cooperating node with relatively lower speed. Figure 2 shows the transmitted and received signal. Figure 3 shows the performance of the system when there is no cooperation, meaning, when there is no diversity. The broken curve in red color shows the system performance when there is no CFO. But, the broken curve in green color shows the effect of CFO with value of 0.2 in the system performance. The system performance, for instance, at 40 dB SNR is less that 10-4 when the system is CFO free.

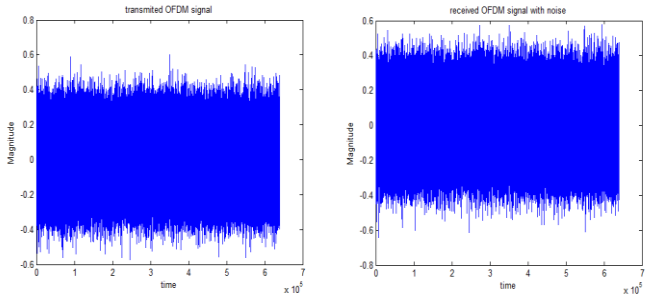

Figure 2: Transmitted and received signal, when there is no cooperation.

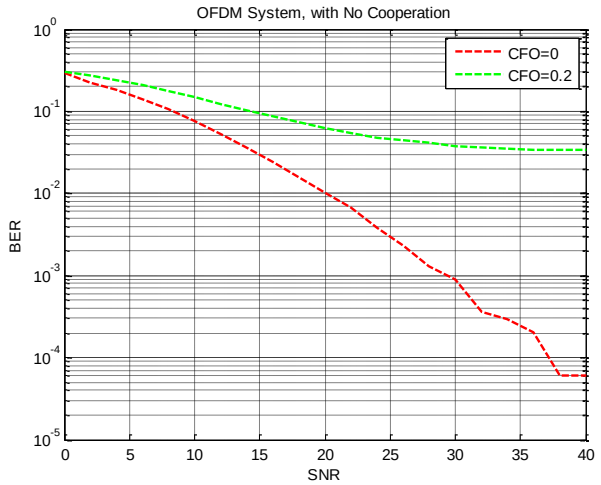

Figure 3: System performance of OFDM system with no cooperation.

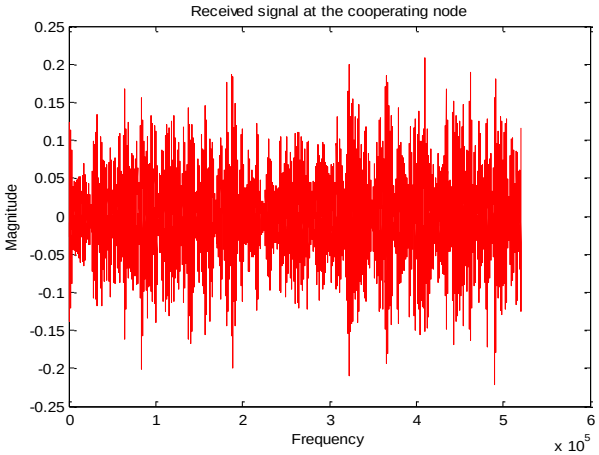

(a)

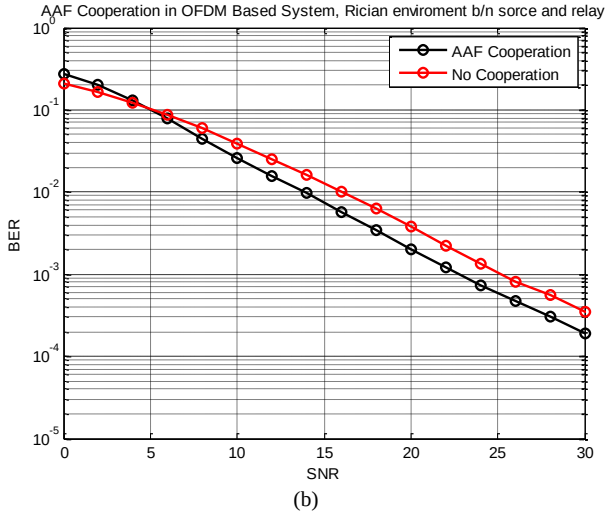

(b)

Figure 4: (a) Signal received at the cooperating node from the source node, 20dB SNR, (b) Ideal OFDM based Cooperative communication system performance

But, the system performance deteriorates to nearly 10^{-1} for the CFO value of 0.2. The Figure 3 shows the bit error rate (BER) deteriorating as the system introduces more carrier frequency offset. However, the system performance should improve when carrier frequency estimation technique is incorporated at the receiver side of the system.

Figure 4a shows the signal received at the cooperating node from the source node and Figure 4b shows the performance of an ideal OFDM based cooperative communication system, where there is no CFO in the system and hence, no need of mitigating the effects of mobility and frequency synchronization error. From the simulation result in Figure 4b, the BER of the system with cooperation improves as the SNR increases starting from 5 dB. Hence, it can be concluded that at higher level of SNR cooperation results in a very improved system performance in terms of BER.

Figure 5 shows the effects of carrier frequency offset (CFO) deteriorating the performance of OFDM based second-order diversity cooperative communication system. Therefore, maximum likelihood estimation developed in the above session in chapter three to mitigate the effects of CFO is used to soothe the severity of CFO in the system. The simulation result shows how the system performance deteriorates for CFO = 0.2.

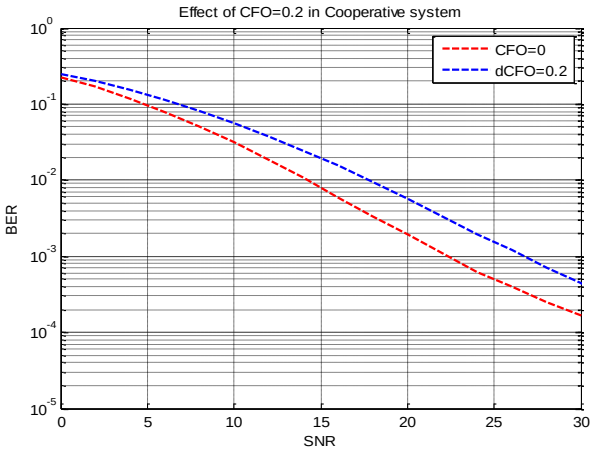

Figure 5: OFDM based cooperative system with CFO effects for CFO=0.2.

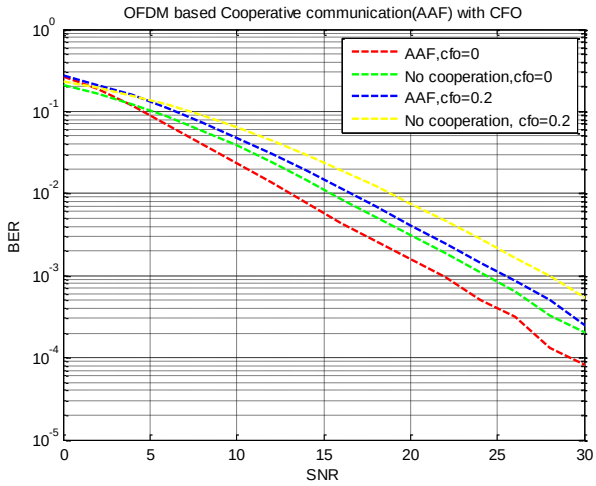

Figure 5: ML estimation of CFO in cooperative communication system.

Figure 6 shows how the integration of ML estimation into the system improved the system performance. The simulation result compares the performance of the system with and without cooperation for CFO values of 0 and 0.2. The performance of the system with AAF cooperation in the environment where 0.2 carrier frequency offset introduced to the system has nearly the same performance with the system without cooperation and carrier frequency offset value of 0. This result shows how cooperation in wireless communication systems can significantly improve the performance in terms of BER against SNR.

VI. Validation of the Simulation Results

The simulation results in Figure 7 and Figure 8 show how the performance of developed cooperative communication system with ML estimation technique overrides the performance obtained from cooperative communication system with self-cancellation (SC) estimation technique.

The comparison between the ML estimation technique and the SC estimation technique is made for CFO values of 0.15, and 0.3 and for modulation types of QAM-4, and QAM-16. In all of the simulation scenarios ML estimation and compensation techniques have shown better performance. The maximum likelihood method gives the best overall results.

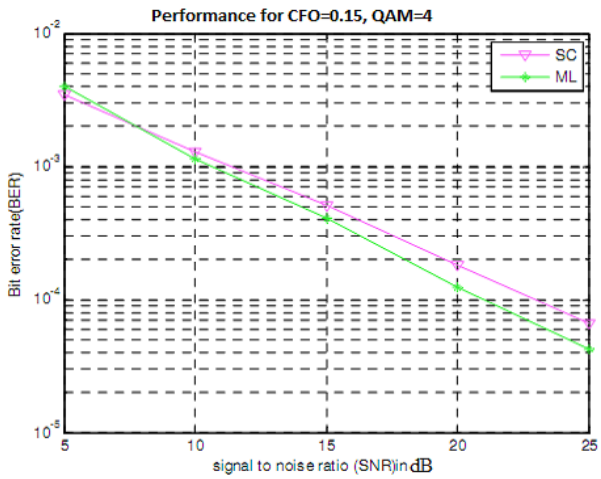

Figure 7: Comparison of ML with SC for CFO= 0.15and 4-QAM

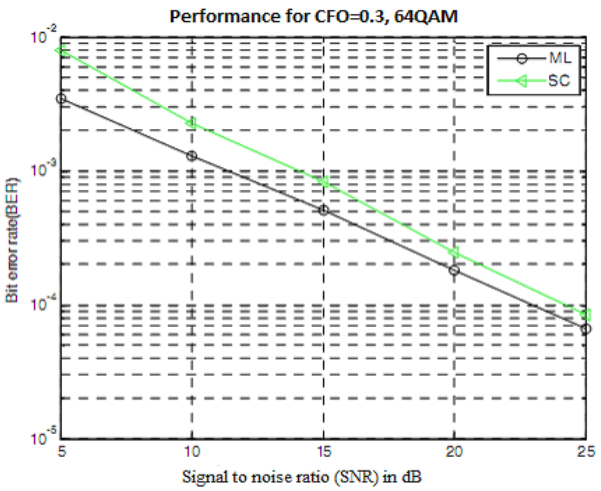

Figure 8: Comparison of ML with SC for CFO=0.3 and 64-QAM.

Figure 7 shows simulation result of the cooperative communication systems based on ML and SC methods for carrier frequency offset value of 0.15 and 4-QAM modulation. The purple colored curve represents the performance curve of cooperative system with self cancellation CFO estimator and the green colored curve represents the performance of cooperative system with maximum likelihood CFO estimator. For these carrier frequency offset value and modulation type, the two methods showed nearly the same performance for SNR values of up to 10 dB. But, thence the performance obtained from the ML method showed better performance in terms of BER.

For CFO value of 0.3 and modulation scheme of QAM-64, the ML based cooperative system shows better performance for the entire range of SNR values. This is shown in Figure 8.

Hence, the system developed in this paper shows better performance when it is compared with the widely studied and previously developed OFDM based cooperative communication systems.

VII. CONCLUSION

The paper considered the most practical scenarios in cooperative communication systems where the cooperating node gets line-of-sight signal from the source node. It has also investigated the effects of carrier frequency offset in amplify and forward cooperative communication system and how these effects are mitigated by using multi-carrier transmission along with maximum-likelihood estimation of CFO. The simulation results of the developed structure have also proved that better BER can be achieved if the cooperating node is restricted to be in a limited range of distance from the source node.

REFERENCES

[1] O. Shin, A. M. Chan, H. T. Kung, and V. Tarokh: "Design of an OFDM cooperative space-time diversity system," *IEEE Trans. Veh. Technol.*, vol. 56, pp. 2203–2215, 2007.

[2] X. Li, F. Ng, and T. Han: "Carrier frequency offset mitigation in asynchronous cooperative OFDM transmissions," *IEEE J. Sel. Areas Commun.*, vol. 56, pp. 675–685, 2008.

[3] Z. Cao, U. Tureli, and Y. D. Yao: "Deterministic multiuser carrier frequency offset estimation for interleaved OFDMA uplink," *IEEE Trans. Commun.*, vol. 52, pp. 1585–1594, 2004.

[4] Y. Zhao and S. Häggman: "Inter Carrier Interference Self Cancellation Scheme for OFDM Mobile Communication Systems," *IEEE Transactions on Communications*, vol. 49, no. 7, pp 1185-1191, 2001.

[5] A. Sendonaris, E. Erkip, and B. Aazhang: "User cooperation diversity. part I. system description," *IEEE Transactions on Communications*, vol. 51, no. 11, pp. 1927–1938, 2003.

[6] A. Nosratinia, T. E. Hunter, and A. Hedayat: "Cooperative communication in wireless networks," *Communications Magazine, IEEE*, vol. 42, no. 10, pp. 74–80, 2004.

[7] J. N. Laneman and G. W. Wornell: "Distributed space-time-coded protocols for exploiting cooperative diversity in wireless networks," *IEEE Trans. Inf. Theory*, vol. 49, pp. 2415–2425, 2003.

[8] B. Gui and L. J. Cimini, Jr.: "Bit loading algorithms for cooperative OFDM systems," *EURASIP Jl. on Wireless Commun. and Networking*, vol.2008, article ID 476797, 9 pages, 2008. doi:10.1155/2008/476797.

[9] B. Gui, L. J. Cimini Jr., L. Dai: "OFDM for cooperative networking with limited channel state information," *IEEE MILCOM'06*, pp. 1-6, 2006.

[10] L. Dai, B. Gui, L. J. Cimini Jr.: "Selective relaying in OFDM multihop cooperative networks," *IEEE WCNC'2007*, pp. 963-968, 2007.

[11] A. Jamshidi, M. Nasiri-Kenari, A. Taherpour: "Outage probability analysis of a coded cooperative OFDM system in multipath Rayleigh fading channels," *IEEE PIMRC'2007*, pages 1-6, 2007.

[12] X. Li, F. Ng, T. Han: "Carrier frequency offset mitigation in asynchronous cooperative OFDM transmissions," *IEEE Trans. Signal processing*,vol. 56, no. 2, 675-685, 2008.

[13] D. Sreedhar and A. Chockalingam: "Interference mitigation in cooperative SFBC-OFDM," *EURASIP Jl. on Advances in Sig. Proc.: Spl. Iss. On Wireless Cooperative Networks*, vol. 2008, article ID 125735, 11 pages, doi:10.1155/2008/125735.

[14] S. Weinstein and P. Ebert: "Data Transmission By Frequency-Division Multiplexing Using the Discrete Fourier Transform" *IEEE Trans. on Commun*. vol. 19 Issue: 5, pp.628 –634, 1971.

[15] Ali Ramadan M. Ali. "Channel Estimation and ICI Cancelation for Adaptive OFDM Systems in Doubly Selective Channel" *Otto-Von Guerickle University*, 2010.

[16] P. H. Moose, "A Technique for Orthogonal Frequency Division Multiplexing Frequency Offset Correction," *IEEE Trans. on Communications*, vol. 42, no. 10, pp. 2908-2914, 1994.

[17] J-J. van de Beek, M. Sandell, and P. O. Börjesson: "ML Estimation of Time and Frequency Offset in OFDM Systems," *IEEE Trans. on Signal Processing*, vol.45, no. 7, pp. 1800-1805, 1997.

ISSN 1805-5443